

COAGULATION

Targeted clinical control of trauma patient coagulation through a thrombin dynamics model

Amor A. Menezes,^{1,2} Ryan F. Vilardi,³ Adam P. Arkin,^{1,2,4*} Mitchell J. Cohen^{5,6*}2017 © The Authors,
some rights reserved;
exclusive licensee
American Association
for the Advancement
of Science.

We present a methodology for personalizing the clinical treatment of severely injured patients with acute traumatic coagulopathy (ATC), an endogenous biological response of impaired coagulation that occurs early after trauma and shock and that is associated with increased bleeding, morbidity, and mortality. Despite biological characterization of ATC, it is not easily or rapidly diagnosed, not always captured by slow laboratory testing, and not accurately represented by coagulation models. This lack of knowledge, combined with the inherent time pressures of trauma treatment, forces surgeons to treat ATC patients according to empirical resuscitation protocols. These entail transfusing large volumes of poorly characterized, nontargeted blood products that are not tailored to an individual, the injury, or coagulation dynamics. Massive transfusion mortality remains at 40 to 70% in the best of trauma centers. As an alternative to blunt treatments, time-consuming tests, and mechanistic models, we used dynamical systems theory to create a simple, biologically meaningful, and highly accurate model that (i) quickly forecasts a driver of downstream coagulation, thrombin concentration after tissue factor stimulation, using rapidly measurable concentrations of blood protein factors and (ii) determines the amounts of additional coagulation factors needed to rectify the predicted thrombin dynamics and potentially remedy ATC. We successfully demonstrate *in vitro* thrombin control consistent with the model. Compared to another model, we decreased the mean errors in two key trauma patient parameters: peak thrombin concentration after tissue factor stimulation and the time until this peak occurs. Our methodology helps to advance individualized resuscitation of trauma-induced coagulation deficits.

INTRODUCTION

Trauma is the leading cause of death and disability between the ages of 1 and 44 (1), with bleeding contributing to the vast majority of these deaths (2). Such hemorrhage is a clinical problem that is complicated by an endogenous biological response called acute traumatic coagulopathy (ATC) (3). ATC results in impaired coagulation, increased bleeding, greater transfusion needs, and a fourfold increase in mortality (3). After the initial phase of hypocoagulability, ATC patients often dynamically transition to a hypercoagulable thrombotic state manifested by excessive clotting (3). The resulting deep vein thrombosis, myocardial infarction, stroke, and organ failure (4) all contribute to an extremely poor outcome in patients who survive their initial injuries.

Despite considerable research (4) on the molecular mechanisms of ATC, there remains a mechanistic and predictive knowledge gap that stems from an inadequate understanding of coagulation mechanisms after an injury and a lack of adequate prediction and real-time decision support for clinicians who care for the severely injured. These failings impede improvements to urgent resuscitation. Thus, there is a need to characterize coagulation mechanisms in trauma patients and to use this characterization to improve the precision of individual treatments.

In the absence of dynamic diagnostics and decision support, current trauma resuscitation practices (4) center on the nontargeted repair of the coagulation cascade (5) (Fig. 1A) and the production of its principal protein thrombin through the transfusion of large vol-

umes of poorly characterized fresh-frozen plasma containing multiple clotting proteins and inhibitors in concentrations that vary from unit to unit. These urgent-care therapies indiscriminately actuate many interacting elements of the coagulation process, resulting in variable untargeted treatment for every patient and with every administration, which is further exacerbated by a lack of clarity about treatment effects on the patient's physiological and biological trajectories resulting from the missing diagnostics and decision support. Such blunt treatment is often either not enough (ATC and bleeding continue) or too much (thrombosis occurs). Both of these extremes contribute to dysregulated inflammation and poor outcomes (4). The mortality from massive transfusion remains at 40 to 70% in the best of trauma centers (6). Retrospective (7) and prospective (8) studies connect the blunt addition of fresh-frozen plasma to poor outcomes, even when the plasma is augmented with empiric ratios of platelets and red blood cells. Transfusion of fresh-frozen plasma is independently associated with a higher risk of multiple organ failure and poor outcomes in patients with hemorrhagic shock (9). Meanwhile, individual interventions consisting of personalized blood protein factor concentrations that are tailored to specific clotting perturbations have been shown to be beneficial (4), although no consensus yet exists on the amount and type of coagulation factors to administer. There is, however, a clinical desire for specific blood products to treat trauma coagulopathy (10). In sum, in an era of increasing personalized medicine, there is an urgent need for targeted, patient-specific trauma coagulation therapies.

Current diagnostics and decision support suffer from a dearth of patient-specific coagulation measurements. Although clinical practice uses several global markers [international normalized ratio (INR), partial thromboplastin time (PTT), prothrombin time (PT), platelet count, fibrinogen concentration, etc.] to diagnose the presence of ATC, these conventional coagulation tests are not enough to tailor a specific intervention and support only the decision to administer plasma or not. Cell-based viscoelastic tests are insufficiently predictive, and their use in resuscitation algorithms also results in nontargeted treatment. Moreover,

¹California Institute for Quantitative Biosciences at University of California, Berkeley, 2151 Berkeley Way, Berkeley, CA 94704–5230, USA. ²Environmental Genomics and Systems Biology Division at E. O. Lawrence Berkeley National Laboratory, 1 Cyclotron Road, Mailstop 955-512L, Berkeley, CA 94720, USA. ³Department of Laboratory Medicine, University of California, San Francisco, 505 Parnassus Avenue, San Francisco, CA 94143, USA. ⁴Department of Bioengineering, University of California, Berkeley, 2151 Berkeley Way, Berkeley, CA 94704–5230, USA. ⁵Department of Surgery, Denver Health Medical Center, 777 Bannock Street, Denver, CO 80204–0206, USA. ⁶Department of Surgery, University of Colorado, 12631 East 17th Avenue, C-305, Aurora, CO 80045, USA. *Corresponding author. Email: aparkin@lbl.gov (A.P.A.); mitchell.cohen@dhha.org (M.J.C.)

Figure S1 diagrams our process for developing a model of the dynamical system that produces thrombin. We used an assay that measures the thrombin dynamical system in a way that is suitable for control-theoretic analysis. The calibrated automated thrombogram (CAT) (15) is a fluorogenic assay that measures the time history of thrombin generation in a blood sample upon the addition of (typically 5 pM) tissue factor (Fig. 2, A and B). All CATs have an initial time delay, followed by a peak response of thrombin concentration that decays to zero. Four parameters describe a CAT trajectory: its displayed time delay (T), its peak thrombin concentration value (P), the time at which this peak occurs (T_p), and the area under the CAT curve that indicates the total thrombin produced (IIa_{tot}).

The CAT is a useful tool (16), but it, like viscoelastic tests, is too time-consuming to be useful for urgent care; the assay takes at least 40 min to measure and nearly an hour to complete. Even early termination of the procedure after 10 min (which does not fully accommodate the completion of the most severely delayed thrombin peak responses) is not fast enough to provide a clinician with coagulation data in the time it takes to wheel a patient to the operating room. In addition, thrombin concentration alone is an uninformative output measure that delivers only an approximation of mechanistic clotting and the coagulation milieu driving observed dynamics, without providing information to a trauma clinician about protein factor targets for patient-specific treatment. In practice, the CAT is currently used only as a research tool or clinically as a Boolean indicator of the necessity of patient coagulation improvement (based primarily on the location of patient P and T_p compared to a surgeon's estimate of normal P and T_p). CAT output is one of several measures (such as PT, PTT, and INR, which together also indicate an ongoing propensity for excessive bleeding or clotting) that are combined with other patient variables and surgeon experience to offer an educated guess of future clotting behavior. An *in silico* dynamical system model that speedily and accurately replicates CAT thrombin concentration output from the rapidly measurable blood protein factor concentration values may enhance the tool's current clinical usefulness by supplying and even leveraging model-based dynamic information.

RESULTS

Patient characteristics

Our study used 20 plasma samples with all of their protein factor concentrations within normal ranges, and we also used the blood of 40 severely injured trauma patients (whose characteristics are in tables S1 and S2), which was drawn at the time when each patient was admitted to San Francisco General Hospital. Among these samples (tables S3 and S4), 37 of 40 samples had a factor deficiency of more than 10% of the respective factor concentration of control mean plasma, 31 of 40 samples had a factor excess of more than 10% of the respective factor concentration of control mean plasma, 32 of 40 samples had a factor deficiency of more than 1 SD below the respective factor concentration mean of the 20 normal plasma samples, and 39 of 40 samples had a factor excess of more than 1 SD above the respective factor concentration mean of the 20 normal plasma samples.

Measurement of the thrombin dynamical system

Figure 2C shows *in vitro* CATs that were generated from the 20 normal and 40 trauma plasma samples. Most of the trauma CATs in the sample have $P > 0.2 \mu\text{M}$, with peaks that surpass the aggregate peak of the normal CATs (this means that most trauma CATs in the

sample are “thrombotic”), although a few have lower peaks (these CATs are “hemorrhagic”). Figure 2D illustrates common trends in the CAT parameters of normal and trauma patients. Distinguishing between these two patient classes with linear classifiers is problematic because of an overlap between normal and trauma CAT parameters, which means that the two groups are not separated in CAT parameter space. Additional computational approaches (Supplementary Materials and Methods) reinforce this problematic classification (figs. S2 and S3 and table S5). It can be assumed that the aforementioned CAT measures do not fully capture all curve information. This assumption is validated in this paper because two alternate sets of curve measures are developed to better exploit a CAT, with these two sets being a transformation of each other. Model-free machine learning techniques applied to the measured factor concentrations (Supplementary Materials and Methods) are also uninformative (figs. S4 and S5 and table S6). Figure 2E demonstrates the difficulty of directly applying the coagulation model (11) for trauma using the measured factor concentrations (implementation details are in Supplementary Materials and Methods and table S7), because the model's simulated predictions of P and T_p when compared to the trauma patient data have a mean percent error of 57 and 204%, respectively.

Supplementary Materials and Methods provide methodological background on the form (figs. S6 to S8 and table S8) of a suggested linear time-invariant dynamical system model that can be fit (fig. S6G) nearly perfectly to CAT trajectories. Despite not being mechanistically derived, an alternative method interpretation in Supplementary Materials and Methods is also a phenomenological model that captures the mechanisms of the coagulation cascade in Fig. 1A by simplifying it to Fig. 1B. Our model is further developed next.

Model determination: Identifying a thrombin dynamical system model

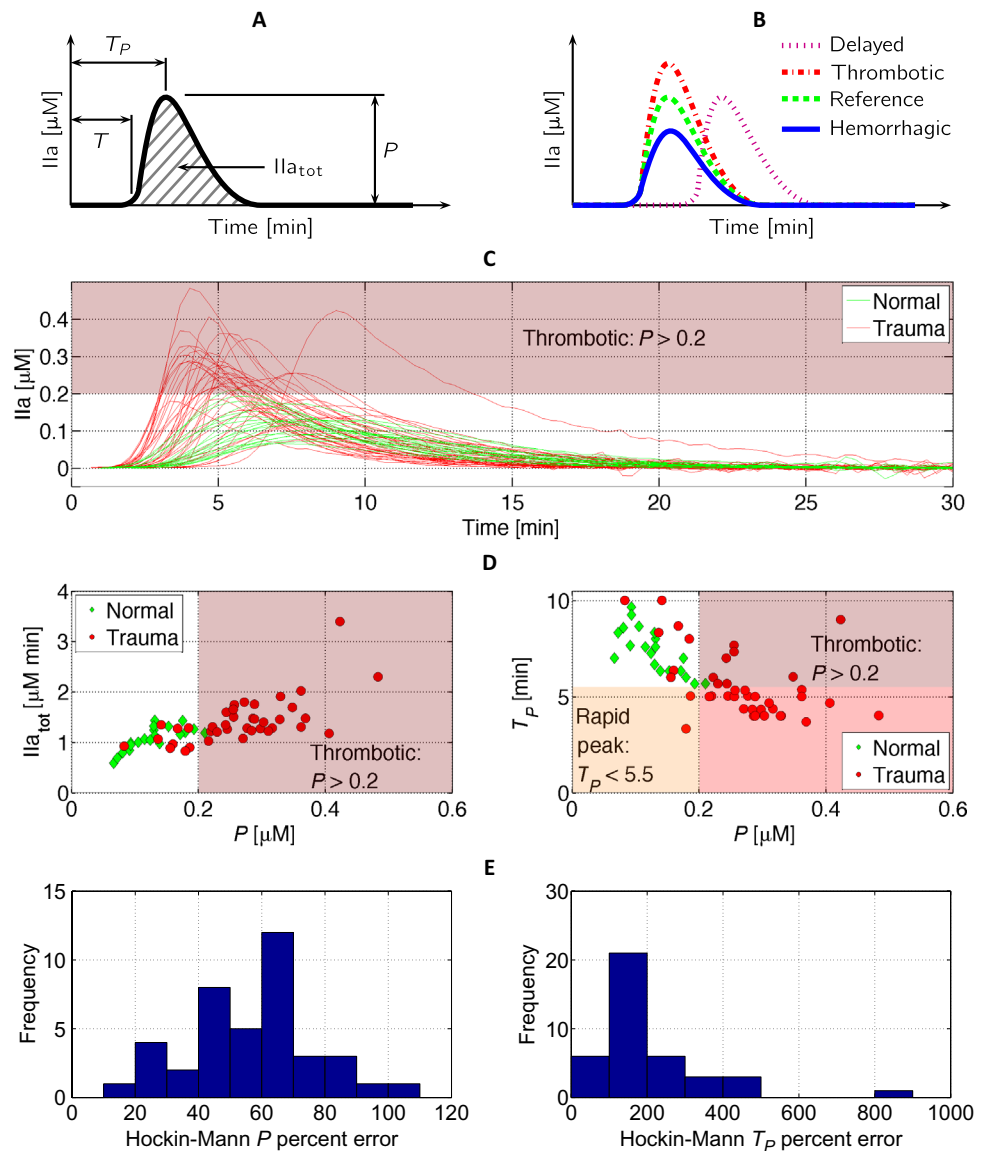
Thrombin concentration over time may be viewed as the single output $y(t)$ of a linear time-invariant dynamical system, which takes tissue factor concentration as a single input $u(t)$ and which has dynamics dominated by the concentrations of factors II, V, VII, VIII, IX, X, and antithrombin III (ATIII; Fig. 1A). In the frequency domain, the dynamical system output becomes $Y(s)$ after applying the Laplace transform to $y(t)$. The tissue factor that initiates coagulation in a blood sample until its quick depletion at CAT start may be considered an impulse input that is applied to the thrombin dynamical system. Thus, $y(t)$ and $Y(s)$ are equivalent to the impulse response of the system in the time and frequency domains, respectively, that is caused by the respective impulse input $u(t)$ or $U(s)$ (for example, a 5 pM impulse at $t = 0$ min). A transfer function (17) model from tissue factor concentration (pM) to thrombin concentration (μM) with time delay T is

$$\frac{Y(s)}{U(s)} = \frac{b}{s^3 + a_2s^2 + a_1s + a_0} e^{-sT} \quad (1)$$

Five parameters have to be identified: a_2 , a_1 , a_0 , b , and T . The transfer function without time delay in Eq. 1 is strictly proper, and the degree of the denominator of this transfer function without time delay (in other words, the degree of the “characteristic polynomial,” which is three) indicates that a differential equation representation of the system has three states. The five parameters of Eq. 1 may be determined for each of the 20 normal and 40 patient CATs with a near-perfect nonlinear least-squares fit (fig. S6G) of the system's

Fig. 2. CAT overview, data set CATs, and trauma-CAT prediction performance by another model.

(A) A CAT displays thrombin concentration over time after a plasma sample has been stimulated by tissue factor. A typical plot indicates a time delay T that precedes the initiation of the thrombin concentration peak response, a peak thrombin concentration value P at time T_P , and the total thrombin produced during clotting, Ia_{tot} . (B) A CAT can also indicate delayed clotting, overclotting (a thrombotic condition), or underclotting (a hemorrhagic condition) when compared to a reference normal plot. (C) The CATs of 20 different lots of plasma having all factor concentrations within a normal range and the CATs of 40 trauma patients admitted to San Francisco General Hospital (table S1 summarizes patient characteristics). All CATs were generated from blood sample stimulation with 5 pM tissue factor. The trauma CATs show pronounced variability in T , P , T_P , and Ia_{tot} . Most of these trauma CATs are thrombotic when compared to the normal CATs, using a definition for a thrombotic CAT as a CAT that has a P value that exceeds an upper bound of normal P (here, defined as $P > 0.2$). If a thrombotic CAT is instead defined with respect to the average normal P , then 39 of the 40 trauma CATs are thrombotic. (D) Plotting normal and trauma patient CAT data together reveals common trends and suggests the possibility of distinguishing between normal and trauma CATs using linear classifiers in the parameter space. However, this approach misclassifies some hemorrhagic CATs as normal and some normal CATs as trauma because of a lack of separation between the two groups in parameter space. (E) Predictions made by the Hockin-Mann model of clotting activity (11) for trauma coagulation from measured factor concentrations have substantial mean error in P and T_P for the 40 trauma patients (57 and 204%, respectively). Implementation details are in Supplementary Materials and Methods.



impulse response using MATLAB Simulink and the trust region-reflective algorithm of the Simulink Design Optimization (SDO) toolbox. A linear relationship exists between all identified b and a_0 (fig. S6H), which means that $b = Ka_0$, where K is a constant. This linear relationship indicates that Eq. 1 includes a traditional, four-parameter, third-order system:

$$\frac{Y(s)}{U(s)} = \left(\frac{K_p}{s+p} \right) \left(\frac{\omega_n^2}{s^2 + 2\zeta\omega_n s + \omega_n^2} \right) e^{-sT} \quad (2)$$

which is the product of a first-order system “low-pass filter” with time constant $1/p$ and gain K and a second-order system with natural frequency ω_n and damping ratio ζ . The damped frequency may be taken to be $\omega_d = \omega_n \sqrt{1 - \zeta^2}$. Defining $\sigma = \zeta\omega_n$ (that is, $\omega_n^2 = \sigma^2 + \omega_d^2$), we let $A = \frac{Kp\omega_n^2}{p^2 - 2\zeta\omega_n p + \omega_n^2}$; $B = \frac{-Kp\omega_n^2}{p^2 - 2\zeta\omega_n p + \omega_n^2}$; $C = \frac{Kp\omega_n^2(p - 2\zeta\omega_n)}{p^2 - 2\zeta\omega_n p + \omega_n^2}$, and

$D = \left(B \cos(\omega_d(t - T)) + \frac{C - \sigma B}{\omega_d} \sin(\omega_d(t - T)) \right)$. Thus, each fitted delayed CAT unit impulse response is given by

$$y(t) = \begin{cases} 0 & \text{if } t < T \\ \left(A e^{-p(t-T)} + D e^{-\sigma(t-T)} \right) 1(t - T) & \text{if } t \geq T \end{cases}$$

for some p , ζ , ω_n , and T computed from a_2 , a_1 , a_0 , and T . The thrombin dynamical system can be thought of as comprising two subsystems, where the first subsystem outputs damped oscillations of a natural frequency and the second subsystem filters these damped oscillations above a cutoff frequency p .

The roots of the characteristic polynomial of Eqs. 1 and 2 are the “poles” of the thrombin dynamical system; if roots of the numerator in Eqs. 1 and 2 existed, these would be the “zeros” of the thrombin dynamical system. Together with the gain, K , the poles and zeros characterize a system’s input-output transfer function, and they

correspondingly also characterize the dynamics represented by the underlying differential equations. When the poles are in the open left half of the complex plane, a dynamical system’s response is stable; the system produces an output that is bounded for any bounded input. Figure 3 (A and B) presents the poles of the fitted 20 normal and 40 patient transfer functions without time delay, respectively. All of these transfer functions have a pair of stable complex conjugate poles as well as a stable pole located on the real axis, in accordance with the pole diagram in Fig. 3C. Thus, p represents the value of the pole on the real axis, and σ and ω_d represent the value of the real and imaginary parts of the complex conjugate pole pair, respectively. An equivalent characteristic polynomial of the transfer function without time delay in Eq. 2 is therefore

$$s^3 + (2\sigma + p)s^2 + (\sigma^2 + \omega_d^2 + 2\sigma p)s + (\sigma^2 + \omega_d^2)p = s^3 + (2\zeta\omega_n + p)s^2 + (\omega_n^2 + 2\zeta\omega_n p)s + \omega_n^2 p \quad (3)$$

Poles and zeros may be located anywhere in the complex plane, but their locations yield qualitative insights into the response of a dynamical system. Figure 3 (A and B) shows that all complex conjugate pole pairs of fitted thrombin dynamical systems are located at various distances along the same two lines at a fixed angle to the real axis, no matter the patient or type of injury. This implies that the coagulation dynamical system is the same in normal and trauma patient plasma, with any observed parametric differences caused by differences in factor concentrations. As a result of the fixed angular locations, all thrombin dynamical systems have fixed $\tan^{-1}(\omega_d/\sigma)$, which is the angle made with the real axis by the complex poles that have a negative imaginary part, equal to fixing the damping ratio ζ . Thus, when

inferring a patient’s thrombin dynamical system from factor concentrations measured in a blood sample upon hospital admittance, inferring p and ω_n and fixing ζ are fruitful. The effect of K , p , ω_n , and T on $y(t)$ is diagrammed in fig. S7 for a reference trajectory that has transfer function values of the averages of K , p , ω_n , ζ , and T of the fitted normal CAT transfer functions. The effects of changing a_2 , a_1 , a_0 , and b are also depicted.

With fixed ζ and Eq. 3, $\zeta \approx c \approx \frac{\sigma}{\omega_n} = \frac{\frac{a_2-p}{2}}{\sqrt{\frac{a_0}{p}}}$, or alternately, $\frac{(a_2-p)^2}{4} \approx c^2 \frac{a_0}{p}$. This implies that an approximation of p is the real root of the cubic equation $p^3 - 2a_2p^2 + a_2^2p - 4a_0c^2 = 0$, which suggests that p is affected by a_2 and a_0 , not a_1 . Also, $\omega_n \approx \frac{a_1p-a_0}{2cp^2}$, which suggests that ω_n is affected by all three of a_2 , a_1 , and a_0 . These expressions for p and ω_n map a temporal interpretation of coagulation to a control-theoretic representation. As will be described below, a_2 , a_1 , and a_0 are tuned with the concentrations of various protein factors in the thrombin dynamical system. This means that the natural frequency ω_n of the second-order subsystem is also tunable, as is the cutoff frequency p of the first-order filter. The thrombin regulation problem is thus one of tuning these two subsystems.

Model construction and parameter estimation: Tuning the thrombin dynamical system

We added the effects of protein factor concentrations to build up our model. Increasing individual protein factor concentrations in normal plasma samples and observing the corresponding CATs informed us of the effect of protein factor “actuators” in controlling normal coagulation. By virtue of the striking similarity between normal and trauma control-theoretic parameter behaviors in Fig. 3 (A and B), we assumed that stimulating normal plasma would also similarly actuate trauma

plasma. Exact replication of observed CAT behavior by control-theoretic parameters should also confirm the determined model’s suitability. Figure 3D data summarizing tables S9 to S11 demonstrate that all candidate actuators are independent and therefore changing a single protein factor concentration does not change any other concentration (as illustrated in fig. S9).

The effects of concentration increases of factors II, VIII, and X (table S12) are of chief interest because factors V and VII are too expensive for practical trauma coagulation control and factors IX and ATIII are too stiff, requiring large concentration increases to alter CATs (table S13). Sample experimental CAT data for concentration increases of factors II, VIII, and X in normal plasma are presented in Fig. 4 (A to C), respectively. Data in Fig. 4D show the CATs of two normal plasma samples that primarily differ only in the concentration of factor V.

When considering CAT alterations that are induced by increases in a protein factor concentration, simulations in Fig. 4 (E to H) and experimental data in figs. S10 to S13 indicate that the effects on

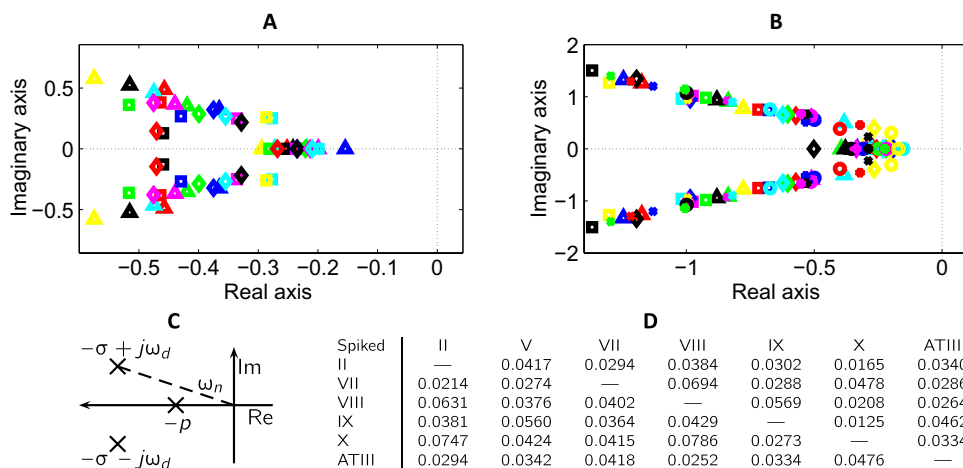


Fig. 3. The structure of the fits of normal and trauma CATs and factor addition independence. (A and B) Poles of the fitted transfer functions without time delay. The three poles of each fit are shown with the same marker and color. The scales of (A) and (B) are proportional so that a line in (A) has the same slope if plotted in (B) and vice versa. (A) All poles of all fits of the 20 normal CATs. (B) All poles of all fits of the 40 patient CATs. (C) The orientation of the three poles for each normal or patient fit. (D) Tabulated normalized means of the SD of protein factor percent activity (columns) after various concentrations of a factor have been spiked into aliquots of a plasma sample (rows), calculated across multiple normal plasma samples ($n = 7$ for factor II at three to seven spikes per sample, $n = 5$ for factor VII at three spikes per sample, $n = 6$ for factor VIII at three to nine spikes per sample, $n = 8$ for factor IX at three to seven spikes per sample, $n = 9$ for factor X at four to six spikes per sample, and $n = 5$ for ATIII at four to five spikes per sample; see table S9). Experimental results in table S10 were normalized by the maximum nonspiked experimental reading for each factor in all plasmas (table S11). The low values here confirm that changing the concentration of a protein factor does not affect the concentration of any other protein factor in the sample with respect to that factor’s total experimental range of movement.

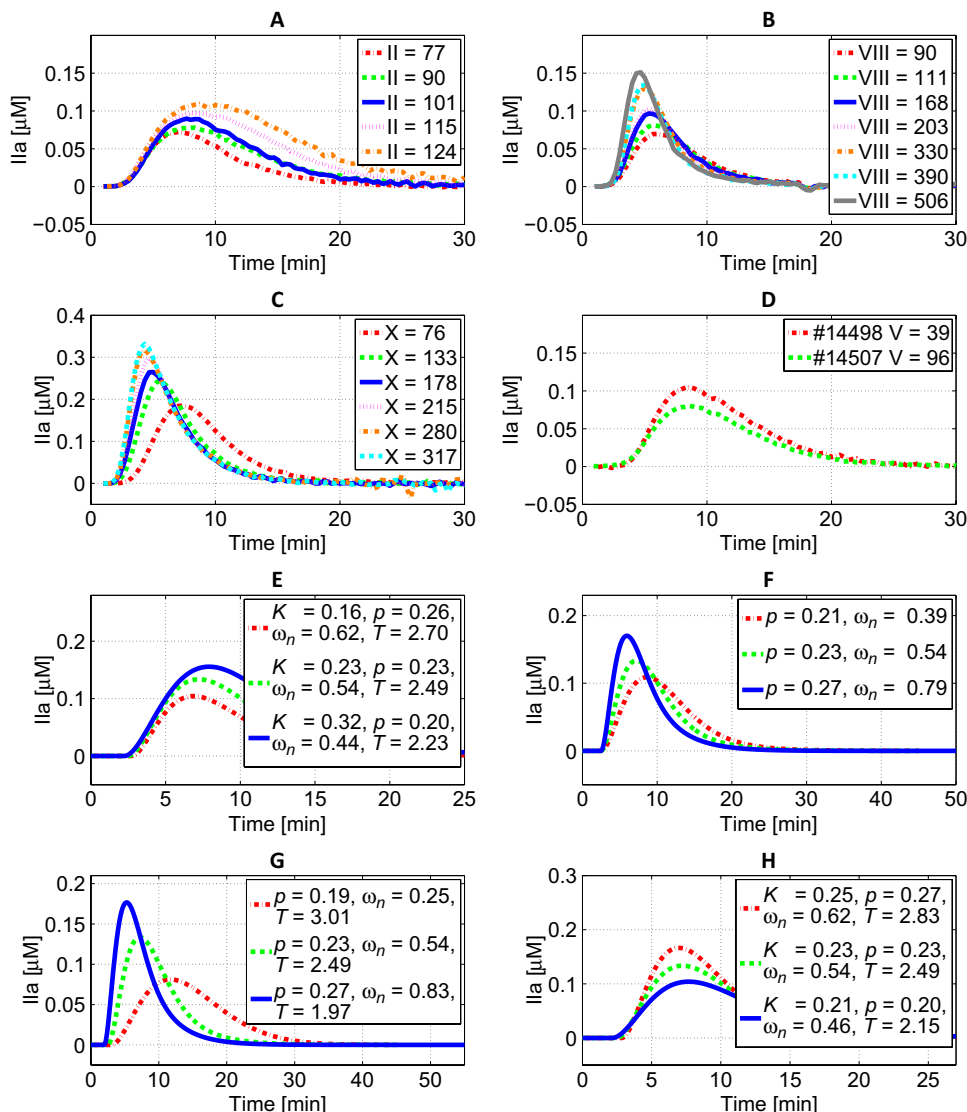


Fig. 4. Emulation of CAT changes induced by factor perturbations. (A) CATs that result from spiking factor II into aliquots of 1 of the 20 normal plasma samples, #14492, to increase that factor's concentration to the values shown. (B) CATs that result from spiking factor VIII into aliquots of 1 of the 20 normal plasma samples, #14492, to increase that factor's concentration to the values shown. (C) CATs that result from spiking factor X into aliquots of 1 of the 20 normal plasma samples, #14504, to increase that factor's concentration to the values shown. (D) The CATs of 2 of the 20 normal plasma samples, #14498 and #14507, which have all factor concentrations except factor V nearly identical. Additional factor perturbation trajectories are in tables S12 and S13. (A to D) Because factor increases cause linear albeit simultaneous effects on the set of four control-theoretic parameters (figs. S10, I to L; S11, I to L; S12, I to L; and S13, I to L), a similar perturbing (in a positive and negative direction) of a reference normal of averaged control-theoretic parameters according to the underlying trends should recapture the CAT effects. (E) Increasing K and decreasing p , ω_n , and T result in trajectories similar to that of increasing factor II in (A). (F) Increasing p and ω_n results in trajectories similar to that of increasing factor VIII in (B). (G) Increasing p and ω_n and decreasing T result in trajectories similar to that of increasing factor X in (C). (H) Decreasing K , p , ω_n , and T results in trajectories similar to that of increasing factor V in (D).

CAT parameters T , P , T_p , and IIa_{tot} , the effects on temporal parameters a_2 , a_1 , a_0 , and b , and the effects on control-theoretic parameters K , p , ω_n , and T are remarkably strongly linear albeit simultaneous. The rationale for choosing control-theoretic parameters instead of temporal parameters as the output of a modeled map from protein factor concentrations is that the set of control-theoretic parameters is the better discriminator, because it achieves differing output trends when inputs

are varied. For instance (fig. S10, E to H), increasing the concentration of factor VIII increases all temporal parameters, and increasing the concentration of factor X causes identical behavior. However, in control-theoretic parameter space, factors VIII and X affect the delay differently; increasing factor X decreases the delay, which is independent of factor VIII (fig. S10L). A second reason for avoiding the temporal parameter space is its small dynamic range with respect to factor II, increases of which cause drastic decreases in already low parameters (fig. S10G) that have a lower bound of zero.

Hence, for the control-theoretic parameter set, it follows from the observed relationships that linear classifiers using factor concentrations can be inferred from all normal and trauma patient data (in other words, there is a sound motivation for linear regression). Although noisy, this approach accounts for patient variability.

Model construction and parameter estimation: Inferring the thrombin dynamical system model

After imposing the average linear effects observed with increasing concentrations of II, VIII, and X in normal plasma, forward stepwise linear regression can be applied to the combined normal and patient data. The method consists of sequentially and greedily adding the linear effect of a blood protein factor concentration measurement (excepting that of II, VIII, and X) that most reduces the error of a least-squares fit to all data for each control-theoretic parameter. This process is repeated until further linear additions of factor concentration measurements no longer significantly improve the fit.

A linear function of the measured initial concentrations of factors II, V, and ATIII predicts K , with absolute errors averaging 25% (SD, 18%). This suggests that inhibitors such as ATIII and activated protein C (Fig. 1A) play a role in tuning the gain. A linear function of the measured initial concentrations of factors II, VIII, X, ATIII, VII, and V predicts p with absolute errors averaging

16% (SD, 14%). The absolute coefficient values are largest for ATIII and II and about equal for VIII, X, VII, and V. This suggests that p is associated with the common pathway. The complex pole pair angle, an alternate measure of the damping ratio, is a constant with mean absolute error of 3.6% (SD, 3.5%). A linear function of the measured initial concentrations of factors II, VIII, X, VII, and V predicts ω_n with absolute errors averaging 41% (SD, 39%). Roughly equal weights on all coefficients

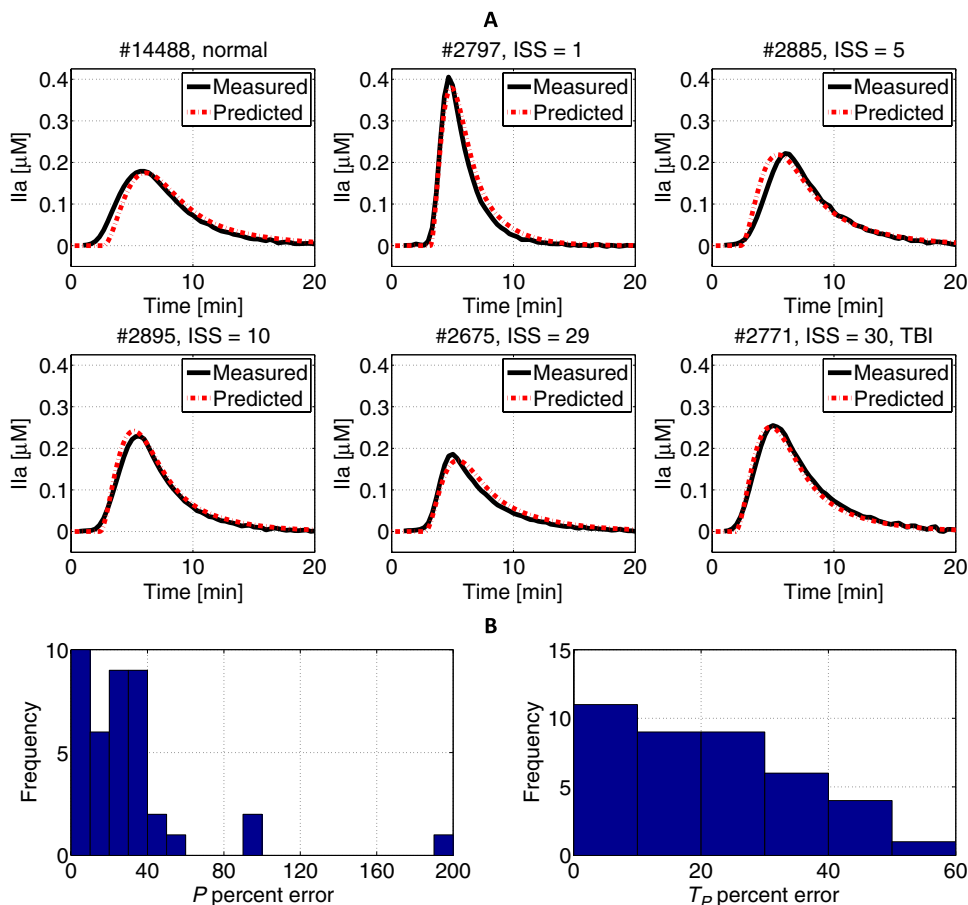


Fig. 5. CAT prediction performance. (A) Best-in-class CAT prediction from protein factor concentrations compared to actual CAT for several different injury classes as measured by ISS: normal plasma sample #14488; low injury severity in trauma patients #2797 and #2885; medium injury severity in trauma patient #2895; high injury severity in trauma patients #2675 and #2771; and TBI is present in trauma patient #2771. (B) The predictive performance for all trauma patients is much improved over (11), regardless of injury (compare to Fig. 2E). Here, mean errors are 31% for P and 22% for T_p .

suggest that ω_n reflects the contact activation and tissue factor pathway effects on the common pathway. Lastly, a linear function of the measured initial concentrations of factors II, X, IX, and V predicts T with absolute errors averaging 22% (SD, 18%). The inferred factor V coefficients are always negative, corroborating Fig. 4H. Fivefold cross-validation on the set of 60 fitted transfer functions to validate the model regression yields mean (for $n = 12$ in the test set) errors having a validation mean (for five test sets) of 39% for P and 17% for T_p . This outcome is comparable to that obtained when inferring with the full data set (Fig. 5).

Thus, given the initial protein factor concentrations in a trauma patient's blood sample at hospital arrival that can be measured within a few minutes, the inferred functions represent a mapping that ultimately determines the temporal parameters in Eq. 1. The thrombin dynamical system can then be simulated to obtain the patient's thrombin CAT response to 5 pM tissue factor input. This process constitutes a low-dimension clinically meaningful trauma coagulation model that averages 0.05 s to compute in MATLAB, which, even with the few minutes required for factor concentration measurement, represents a substantial acceleration from the 40 to 60 min it takes to provide CAT information to a clinician. Figure S14 proposes a clinical workflow.

desirable dynamic changes by adding factors to the blood (factors II, VIII, and X) to attain a “standard” CAT trajectory, a process that would also further validate our model. The clinical implication of predictive factor addition is patient-specific control to potentially achieve desirable coagulation outcomes.

Model prediction: Controlling the thrombin dynamical system

We present an in vitro version of factor addition for patient plasma sample control in two steps. The first step increases factor concentrations in plasma samples and proves an accurate model prediction of changed dynamics, which also experimentally validates our model for non-data set factor concentrations (concentrations that were not used for inference in the previous section). The second step relates to the prediction of concentration additions that achieve a desirable coagulation outcome, taking advantage of the linearity of our model's equations.

For the first step, we took plasma samples for which the model already predicted CATs well (from the original inference data set) and that had sufficient quantity for another assay, spiked in arbitrary amounts of factors II, VIII, and X to randomly increase their

Model prediction: Recapture of known thrombin dynamical systems when deployed as if in clinic

To simulate the CAT response to 5 pM tissue factor input in a patient's blood sample as if in a clinical setting, we used the developed model form and inferred model map to produce temporal and control-theoretic parameters directly from given initial protein factor concentrations (this is unlike the model's development, where these parameters were obtained from fitting normal and patient CATs). The accurate recapture of normal and patient CATs in Fig. 5A from initial protein factor concentrations almost recovers the near-perfect SDO fits to the sample CAT data (such as fig. S6G), data that take 40 min to produce. Accurate CAT recapture in Fig. 5A is independent of the type of trauma injury (as measured by injury severity score or ISS), including traumatic brain injury (TBI). A histogram of the amount of error between our model's predictions and patient data (Fig. 5B) confirms a substantial improvement in trauma CAT prediction on the inference data set over the popular model (Fig. 2E) (11)—the mean percent error in P is 31%, down from 57%, and the mean percent error in T_p is 22%, down from 204%—results that hold up with cross-validation as described above.

Because our model was able to accurately predict CAT dynamics from initial protein factor concentrations, a follow-on question concerned the prediction of

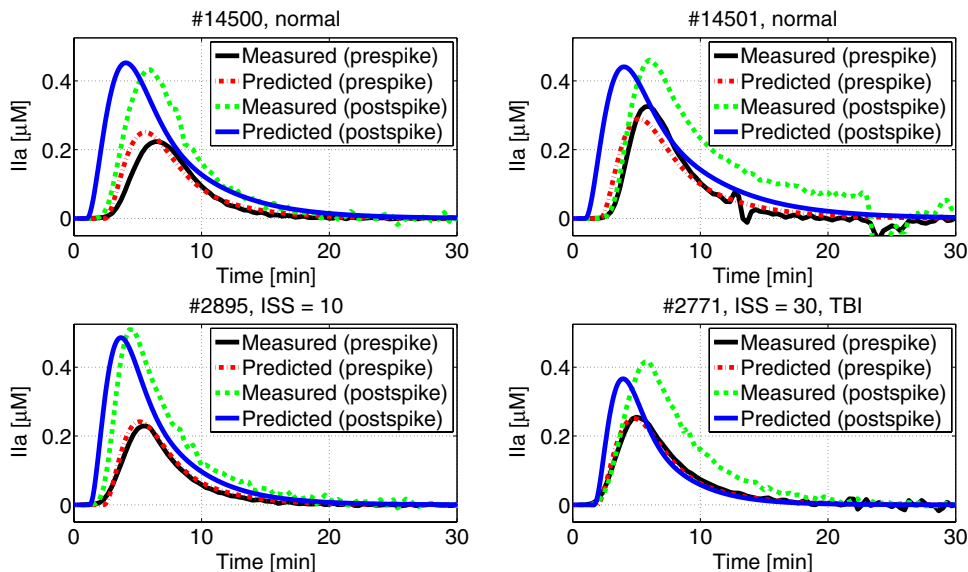


Fig. 6. CAT prediction validation. The CAT prediction from protein factor concentrations compared to the actual CAT for two normal plasma samples #14500 and #14501 and the trajectories from Fig. 5A for two trauma patient samples with available plasma, #2895 and #2771. Arbitrary concentrations of factors II, VIII, and X (table S13) were spiked into each of these four plasma samples. The model was able to capture the postspiking CAT behavior of these samples despite non-data set factor concentrations, although errors in T were the most egregious.

concentrations, and thereafter confirmed the model's continued CAT predictive power after measuring the new factor concentrations in these samples, which were now no longer part of the inference data set. Figure 6 demonstrates successful capture of postspiking trajectory behavior for both normal and trauma plasma samples, with errors in T being the most visible. The implication of the successful CAT capture is that control-theoretic parameters can be accurately predicted by the model even for factor concentrations that are not a part of the inference data set.

For the second step, consider that the internal model equations constitute a system of four equations (for control-theoretic parameters) in seven variables (factor concentrations). If the model is provided with a desirable CAT trajectory, then this provision is equivalent to specifying the four control-theoretic parameters and requiring the model to solve an underdetermined system with fewer equations than unknowns, for which there could be infinitely many solutions if a solution exists. The number of feasible solutions can be reduced by eliminating those that specify decreased factor concentrations (these solutions are not physically realizable), those that are expensive (for example, where a large amount of factor V is called for), and those that are not achievable (because some factors are not available in the emergency room). Hence, predicting increases in concentrations of factors II, VIII, and X that are required to achieve a desirable CAT trajectory amounts to examining the pseudoinverse of the model's linear expressions. In the case of the spiked CATs in Fig. 6, where control-theoretic parameters are accurately predicted by the model from factor concentrations even for non-data set inputs, a solution to the inverse problem of providing control-theoretic parameters and asking for factor concentration increases obviously exists (Fig. 6 is one such feasible solution). That is, if control-theoretic parameters from the measured spiked CAT trajectories of Fig. 6 are provided to the model, then it follows that at least one solution to the linear underlying expressions for factor concentrations is the one from which

the model was previously generating accurate CATs. The successful validation that is shown in Fig. 6 is analogous to asking the model for one combination of protein factor increases that approximate a measured CAT. Thus, Fig. 6 demonstrates the likelihood of the model's ability (at least in vitro) to achieve a standard, desirable CAT trajectory.

DISCUSSION

Trauma-induced coagulopathy is multifactorial and remains incompletely characterized. Despite the emerging importance of fibrinolysis, platelet function, inflammation, etc., hemostatic resuscitation includes the transfusion of either plasma-based or prothrombin complex concentrate-based fluids, with the former primarily containing coagulation factors and the latter including concentrated coagulation factors. Hence, a central charge in trauma resuscitation is to "repair" thrombin-based coagulation through nontargeted factor administration.

This current approach to resuscitative care for a trauma patient relies on protocols that guide the transfusion of large volumes of blood products in a prespecified ratio. These massive-transfusion protocols result in both overresuscitation and underresuscitation depending on the patient characteristics and clinical and biological dynamics. Few patients do well with these nonpersonalized approaches to care, depending on their fit to the nonspecific algorithmic care and to the care team's clinical judgment, which is why massive-transfusion mortality remains at 40 to 70% in the best trauma centers (6). We demonstrate that a control-oriented dynamical systems approach to trauma coagulation results in a simple, accurate, quick, and meaningful model that may eventually be used to personalize resuscitation after trauma. We take advantage of the dynamics of a driver of downstream coagulation, which is thrombin concentration change over time after tissue factor stimulation. We show how the implicit dynamical system can be inferred from concentration measurements of coagulation proteins in a plasma sample that take a few minutes. Our approach reduces the 40- to 60-min time that is required by the CAT assay to measure this thrombin concentration change over time. Our approach is feasible even if a combined assay is not yet commercially available or if the measurements are not currently cheap because the assays should become packaged and inexpensive with more frequent use. With the inferred dynamical system, we then predict and regulate thrombin dynamics.

The patient-specific model developed here captures the dynamics of thrombin generation through a single-input (tissue factor concentration), single-output (thrombin concentration), linear time-invariant dynamical system, which has dynamics that are affected by the concentrations of the rapidly measurable blood protein factors in both normal and trauma patients. The two implications are that the underlying thrombin regulation is the same in both groups and that the complex biochemical reactions underlying thrombin generation combine to create a simple overall dynamical system that is controllable,

for instance, in an open-loop way by changing the concentrations of some of the rapidly measurable blood protein factors. Closed-loop control through tissue factor concentration change is not pursued in this work because, for analytical simplicity, the value of input tissue factor concentration is fixed at the typical 5 pM value that is used by the CAT measurement tool.

We show that the thrombin dynamical system is composed of two subsystems. The first subsystem generates damped thrombin oscillations at some natural frequency, and the second subsystem filters thrombin oscillations above some cutoff frequency. The amount of damping in a thrombin dynamical system always stays constant, regardless of patient or trauma characteristics. Identical behavior in normal plasma suggests that the thrombin dynamical system is the same in a normal person and in a trauma patient, with any observed parametric differences caused by differences in factor concentration. After injury, the dynamical system itself remains the same as it was before injury, without any additional mechanisms that might arise under trauma conditions.

Increasing blood protein factor concentrations tunes the two subsystems; specifically, the oscillation natural frequency and the filter cutoff frequency are affected, as are the thrombin dynamical system gain (output magnification) and the response delay. The implication is that the clinical thrombin regulation problem involves appropriately tuning the two subsystems by changing the subsystem parameters with changes in factor concentrations.

Another interpretation of the two-subsystem oscillation-filter understanding of the thrombin dynamical system is that there are three underlying system states (where the term “states” is meant in a control-theoretic sense) that undergo linear time-invariant dynamics. These three states are thrombin, the Xa-Va complex (prothrombinase), and the complex of tissue factor with VIIa; the latter two complexes are already recognized as clinically important. Just as the oscillation-filter understanding of the thrombin dynamical system is associated with four control-theoretic parameters (oscillation natural frequency, filter cutoff frequency, gain, and delay), four temporal parameters are associated with this equivalent interpretation.

When adding blood protein factor concentrations to the thrombin dynamical system to build up our model, the experimental data indicate that the effects of each factor’s addition are independent; changing the concentration of a protein factor does not affect the concentration of any other protein factor. For practical reasons, we focused on the tuning of factors II, VIII, and X. Strongly linear albeit simultaneous effects are indicated on a set of four CAT parameters, the set of four temporal parameters, and the set of four control-theoretic parameters, with individual parameter effects being more distinguishable on the control-theoretic parameter set than on the temporal parameter set. The demonstrated strongly linear effects motivate forward stepwise linear regression to account for the actions of the other remaining quickly measurable factors V, VII, IX, and ATIII. The resultant linear map from factor concentrations to control-theoretic parameters distinguishes this model from contemporary nonlinear stoichiometry-based models.

The ensuing estimated dynamical system can predict the time history of thrombin concentration in a plasma sample after stimulation by tissue factor more accurately than a popular nonlinear coagulation model, for a variety of trauma conditions, on the data set used for inference (cross-validated here). This estimated dynamical system can also make accurate predictions for non-data set plasma samples. Because of the linearity of the control-theoretic parameter prediction

equations, they can be simply and quickly inverted if control-theoretic parameters for a desired CAT are provided. The pseudoinverse will generate several possibilities of the seven input concentrations to achieve the four stipulated control-theoretic parameters. Future human studies should provide insight into potential clinical impact of these possibilities, with the least expensive possibility chosen in the event of comparably beneficial options. Future guidelines should also specify a desirable CAT profile (or a desirable sequence of profiles) that represents an improved patient outcome for a presented CAT. We have demonstrated the likelihood of our model’s ability (at least *in vitro*) to make this desirable restoration through factor addition.

Five caveats are applicable to this work—two for the proposed trauma treatment methodology and three for the described model. First, because there are no guidelines for either a standard desirable CAT trajectory or an appropriate sequence of trajectories to be achieved by targeted clinical coagulation control to improve a trauma patient’s condition, we only show that we can control clinically and biologically relevant thrombin production, without specifying what the control goal should be. The control goal will have to be chosen to minimize thrombotic risk. Although it has been established elsewhere (4) that affecting coagulation can result in improved survival (and indeed represents the central tenet of current resuscitation protocols), it remains to be experimentally determined and clinically validated whether changing thrombin will result in improved survival.

Second, only *in vitro* control is demonstrated here, and it is expected that the model will need modification for achieving *in vivo* control objectives. Third, this work only investigates the tuning of the thrombin dynamical system with the concentrations of factors II, VIII, and X, leaving the effects of factor concentrations V, VII, IX, and ATIII to inference. It is anticipated that a more comprehensive tuning investigation that includes the missing factors will provide better thrombin predictive insight. Fourth, the overall control authority (thrombin tuning range and tuning capability) that is available with all seven factor concentrations is an open question. Finally, our linear time-invariant model is a local approximation of nonlinear thrombin generation dynamics at an operating point of 5 pM tissue factor concentration, although this value is a standard current experimental practice.

A larger study with more trauma patients that also includes the missing factors is suggested as an immediate next step, to improve the inferred linear estimation equations for control-theoretic parameters and to more fully validate thrombin concentration time-history predictions. Next, it may be desirable to have a thrombin dynamical system model that is valid over the entire input tissue factor concentration range, which will facilitate thrombin concentration closed-loop control by varying tissue factor concentration. Other recommendations for additional research include augmenting the model in this paper to capture the results obtained from measures of functional coagulation that are not thrombin-based (such as viscoelastic testing, a cell-based measure) and to capture platelet function. In the longer term, an improved coagulation model may be integrated into a point-of-care device.

The most important enabler of our analysis was the CAT assay, which, in control theory parlance, provided an impulse response measurement of the underlying thrombin dynamical system. An impulse response completely characterizes a linear time-invariant dynamical system (17). Once we realized that a vital control-theoretic measurement was already in experimental practice through the CAT test, we set out to exploit this information. We had to first show

that linearity and time invariance held for the underlying system. Perhaps unsurprisingly, we found that system linearity was true for a CAT input value that is typically used in experiments, a value that was probably informed by experimental intuition. Thereafter, we applied known system identification ideas, including that of small perturbations, to determine overall system behavior. This process yielded startling linear results for the system's CAT parameters, temporal parameters, and control-theoretic parameters. We believe that our approach is more broadly applicable to pathophysiology and that similar approximations exist for complex biological processes. The chief task is really the identification of a suitable control-theoretic measurement (such as an impulse response or a step response) that can be exploited. It is preferable that this measurement be either already in experimental use or obtainable from test apparatus that can be quickly and cheaply put together.

Factor addition to change undesired thrombin dynamics is a tailored approach to coagulopathy treatment that differs from the current blunt practice of using empiric ratios of blood products and could form the basis for targeted personalized treatment of bleeding after injury. For a specific trauma patient, it will now be possible to outline a sequence of desirable invoked thrombin production trajectories that can be achieved by targeted clinical coagulation control, using the provided thrombin dynamics model.

MATERIALS AND METHODS

Study design

The 40 trauma patient blood samples were randomly selected from among those that were collected by the ongoing Activation of Coagulation and Inflammation in Trauma investigation (which seeks to prospectively characterize drivers of coagulation and outcomes of severe traumatic injury and shock) and had sufficient quantity for at least one experimental assay. Our study was blinded in that patient demographics and outcomes were unknown until the completion of all work that is described in this paper. To construct a model and estimate its parameters, we used a mix of experimental perturbations and computational inference. Five biological replicates were taken when perturbing factor II, 10 biological replicates were taken when perturbing factor VIII, and 10 biological replicates were taken when perturbing factor X. Perturbation experiment outliers were of two types. Either the factor perturbation caused a sample to be so thrombotic that the generated measurement went off the scale and its premature end precluded a fit to this incomplete measurement or the structure of the fit (as depicted in Fig. 3, A and B) differed from that of all 60 unperturbed normal and trauma measurements. Nine of 146 completed measurements of perturbed conditions for the model construction process were such outliers (in other words, only 9 were different from the other 197, consisting of the 137 perturbed and the 60 unperturbed). Before experimental model validation, the patient ISS corresponding to blood samples that had sufficient quantity for another assay were made known, and this was to ensure that the validation samples had different ISSs.

All other materials and methods are provided in the Supplementary Materials and Methods.

SUPPLEMENTARY MATERIALS

www.sciencetranslationalmedicine.org/cgi/content/full/9/371/eaaf5045/DC1

Materials and Methods

Fig. S1. Summary of our model development process.

Fig. S2. Lack of correlation between trauma patient characteristics and outcomes.
 Fig. S3. Overlap of normal and trauma patient classes.
 Fig. S4. Model-free machine learning techniques applied to measured factor concentrations.
 Fig. S5. Lack of correlation between trauma patient characteristics and principal components.
 Fig. S6. Linearity, justification, and fit of a thrombin dynamical system model.
 Fig. S7. Model control-theoretic and temporal parameter effects.
 Fig. S8. K-means classification using control-theoretic parameters.
 Fig. S9. Independence of factor addition to normal plasma.
 Fig. S10. Parameter effects caused by increasing the concentration of factor II, VIII, or X in a sample of normal plasma.
 Fig. S11. Parameter effects caused by increasing the concentration of factor II in five normal plasma samples.
 Fig. S12. Parameter effects caused by increasing the concentration of factor VIII in 10 normal plasma samples.
 Fig. S13. Parameter effects caused by increasing the concentration of factor X in 10 normal plasma samples.
 Fig. S14. Proposed clinical workflow.
 Table S1. Summary of trauma patient characteristics.
 Table S2. Normal and trauma patient plasma sample data (provided as an Excel file).
 Table S3. Closeness of trauma patient factor concentrations to values from control mean plasma.
 Table S4. Closeness of trauma patient factor concentrations to means from 20 normal plasma samples.
 Table S5. Unsuccessful k-means classification of normal and trauma using four CAT dimensions.
 Table S6. Unsuccessful k-means classification of normal and trauma using seven concentrations, equivalent to using the first two and the first three principal components.
 Table S7. Conversion factors used for Hockin-Mann model prediction of trauma CATs.
 Table S8. Thrombin dynamical system linearity testing data (provided as an Excel file).
 Table S9. Factor addition independence testing data (provided as an Excel file).
 Table S10. Mean of the SD of nonspiked factor concentrations across multiple normal plasma samples.
 Table S11. Maximum nonspiked factor concentration in normal plasma samples.
 Table S12. Factor perturbation data (provided as an Excel file).
 Table S13. Ancillary factor perturbation data and model validation data (provided as an Excel file).
 References (18–21)

REFERENCES AND NOTES

1. D. A. Sleet, L. L. Dahlberg, S. V. Basavaraju, J. A. Mercy, L. C. McGuire, A. Greenspan, Injury prevention, violence prevention, and trauma care: Building the scientific base. *MMWR Suppl.* **60**, 78–85 (2011).
2. D. S. Kauvar, R. Lefering, C. E. Wade, Impact of hemorrhage on trauma outcome: An overview of epidemiology, clinical presentations, and therapeutic considerations. *J. Trauma Acute Care Surg.* **60**, S3–S11 (2006).
3. A. Cap, B. Hunt, Acute traumatic coagulopathy. *Curr. Opin. Crit. Care* **20**, 638–645 (2014).
4. E. Gonzalez, H. B. Moore, E. E. Moore, Eds. *Trauma Induced Coagulopathy* (Springer, 2016).
5. R. L. C. Adams, R. J. Bird, Review article: Coagulation cascade and therapeutics update: Relevance to nephrology. Part 1: Overview of coagulation, thrombophilias and history of anticoagulants. *Nephrology (Carlton)* **14**, 462–470 (2009).
6. K. C. Sihler, L. M. Napolitano, Massive transfusion: New insights. *Chest* **136**, 1654–1667 (2009).
7. D. Frith, K. Brohi, Massive transfusion in trauma, in *Transfusion in the Intensive Care Unit*, N. P. Juffermans, T. S. Walsh, Eds. (Springer, 2009), pp. 101–119.
8. J. B. Holcomb, B. C. Tilley, S. Baraniuk, E. E. Fox, C. E. Wade, J. M. Podbielski, D. J. del Junco, K. J. Brasel, E. M. Bulger, R. A. Callcut, M. J. Cohen, B. A. Cotton, T. C. Fabian, K. Inaba, J. D. Kerby, P. Muskat, T. O'Keefe, S. Rizoli, B. R. H. Robinson, T. M. Scalea, M. A. Schreiber, D. M. Stein, J. A. Weinberg, J. L. Callum, J. R. Hess, N. Matijevic, C. N. Miller, J.-F. Pittet, D. B. Hoyt, G. D. Pearson, B. Leroux, G. van Belle, Transfusion of plasma, platelets, and red blood cells in a 1:1:1 vs a 1:1:2 ratio and mortality in patients with severe trauma: The PROPPR randomized clinical trial. *JAMA* **313**, 471–482 (2015).
9. J. L. Johnson, E. E. Moore, J. L. Kashuk, A. Banerjee, C. C. Cothren, W. L. Biffi, A. Sauaia, Effect of blood products transfusion on the development of postinjury multiple organ failure. *Arch. Surg.* **145**, 973–977 (2010).
10. C. Gaarder, A. Holtan, P. A. Naess, Prehospital point-of-care monitoring and goal-directed therapy: Does it make a difference? *J. Trauma Acute Care Surg.* **78**, S60–S64 (2015).
11. M. F. Hockin, K. C. Jones, S. J. Everse, K. G. Mann, A model for the stoichiometric regulation of blood coagulation. *J. Biol. Chem.* **277**, 18322–18333 (2002).
12. K. G. Mann, Is there value in kinetic modeling of thrombin generation? *Yes. J. Thromb. Haemost.* **10**, 1463–1469 (2012).

13. H. C. Hemker, S. Kerdelo, R. M. W. Kremers, Is there value in kinetic modeling of thrombin generation? No (unless...). *J. Thromb. Haemost.* **10**, 1470–1477 (2012).
14. D. Luan, F. Szlam, K. A. Tanaka, P. S. Barie, J. D. Varner, Ensembles of uncertain mathematical models can identify network response to therapeutic interventions. *Mol. Biosyst.* **6**, 2272–2286 (2010).
15. H. C. Hemker, P. Giesen, R. AlDieri, V. Regnault, E. de Smed, R. Wagenvoord, T. Lecompte, S. Beguin, The calibrated automated thrombogram (CAT): A universal routine test for hyper- and hypocoagulability. *Pathophysiol. Haemost. Thromb.* **32**, 249–253 (2002).
16. M. D. Lancé, A general review of major global coagulation assays: Thrombelastography, thrombin generation test and clot waveform analysis. *Thromb. J.* **13**, 1 (2015).
17. C.-T. Chen, *Linear System Theory and Design* (Oxford Univ. Press, 1984).
18. L. Ljung, *System Identification* (Springer, 1998).
19. H. Akaike, A new look at the statistical model identification. *IEEE Trans. Automat. Contr.* **19**, 716–723 (1974).
20. J. Rissanen, Modeling by shortest data description. *Automatica* **14**, 465–471 (1978).
21. J. S. Bay, *Fundamentals of Linear State Space Systems* (McGraw-Hill, 1999).

Acknowledgments: We thank A. Bezzola and L. R. Petzold for sharing their MATLAB implementation of the Hockin-Mann model, we appreciate A. Conroy's assistance in compiling patient data, and we are grateful for manuscript feedback from E. D. Gustafson, A. T. Klesh, and anonymous reviewers. **Funding:** This study was supported by the Department of Defense (DOD W911NF-10-1-0384) and the NIH (1 UM1 HL120877). **Author contributions:** A.A.M., A.P.A., and M.J.C. developed the model; A.A.M., R.F.V., and M.J.C. experimentally validated the model; and A.A.M., A.P.A., and M.J.C. wrote the paper. **Competing interests:** The authors declare that they have no competing interests.

Submitted 12 October 2015
Resubmitted 18 February 2016
Accepted 23 September 2016
Published 4 January 2017
10.1126/scitranslmed.aaf5045

Citation: A. A. Menezes, R. F. Vilardi, A. P. Arkin, M. J. Cohen, Targeted clinical control of trauma patient coagulation through a thrombin dynamics model. *Sci. Transl. Med.* **9**, eaaf5045 (2017).



Targeted clinical control of trauma patient coagulation through a thrombin dynamics model

Amor A. Menezes, Ryan F. Vilarde, Adam P. Arkin and Mitchell J. Cohen (January 4, 2017)
Science Translational Medicine 9 (371), . [doi:
10.1126/scitranslmed.aaf5045]

Editor's Summary

The key to resuscitation is in the blood

In the setting of severe trauma, some patients develop acute traumatic coagulopathy, impaired coagulation that can occur in response to shock. For patients who are already bleeding and then develop coagulopathy, there is no time to carefully perform laboratory analysis, and blood products are usually transfused according to standardized protocols. Because these protocols are not tailored to individual patients or injuries, this can result in insufficient or excessive blood product transfusions, which contribute to the high risk of mortality. Using dynamic modeling, Menezes *et al.* demonstrated a method for calculating each patient's transfusion requirements using only laboratory values that can be easily and quickly obtained in the emergency setting, which should allow for individually tailored resuscitation.

The following resources related to this article are available online at <http://stm.sciencemag.org>.
This information is current as of January 4, 2017.

Article Tools	Visit the online version of this article to access the personalization and article tools: http://stm.sciencemag.org/content/9/371/eaaf5045
Supplemental Materials	"Supplementary Materials" http://stm.sciencemag.org/content/suppl/2016/12/27/9.371.eaaf5045.DC1
Related Content	The editors suggest related resources on <i>Science's</i> sites: http://stm.sciencemag.org/content/scitransmed/8/353/353ra112.full http://stm.sciencemag.org/content/scitransmed/8/365/365ra156.full http://stm.sciencemag.org/content/scitransmed/7/302/302ed11.full http://stm.sciencemag.org/content/scitransmed/7/285/285ra61.full
Permissions	Obtain information about reproducing this article: http://www.sciencemag.org/about/permissions.dtl

Science Translational Medicine (print ISSN 1946-6234; online ISSN 1946-6242) is published weekly, except the last week in December, by the American Association for the Advancement of Science, 1200 New York Avenue, NW, Washington, DC 20005. Copyright 2017 by the American Association for the Advancement of Science; all rights reserved. The title *Science Translational Medicine* is a registered trademark of AAAS.

Supplementary Materials for

Targeted clinical control of trauma patient coagulation through a thrombin dynamics model

Amor A. Menezes, Ryan F. Vilardi, Adam P. Arkin,* Mitchell J. Cohen*

*Corresponding author. Email: aparkin@lbl.gov (A.P.A.); mitchell.cohen@dhha.org (M.J.C.)

Published 4 January 2017, *Sci. Transl. Med.* **9**, eaaf5045 (2017)

DOI: 10.1126/scitranslmed.aaf5045

The PDF file includes:

Materials and Methods

Fig. S1. Summary of our model development process.

Fig. S2. Lack of correlation between trauma patient characteristics and outcomes.

Fig. S3. Overlap of normal and trauma patient classes.

Fig. S4. Model-free machine learning techniques applied to measured factor concentrations.

Fig. S5. Lack of correlation between trauma patient characteristics and principal components.

Fig. S6. Linearity, justification, and fit of a thrombin dynamical system model.

Fig. S7. Model control-theoretic and temporal parameter effects.

Fig. S8. K-means classification using control-theoretic parameters.

Fig. S9. Independence of factor addition to normal plasma.

Fig. S10. Parameter effects caused by increasing the concentration of factor II, VIII, or X in a sample of normal plasma.

Fig. S11. Parameter effects caused by increasing the concentration of factor II in five normal plasma samples.

Fig. S12. Parameter effects caused by increasing the concentration of factor VIII in 10 normal plasma samples.

Fig. S13. Parameter effects caused by increasing the concentration of factor X in 10 normal plasma samples.

Fig. S14. Proposed clinical workflow.

Table S1. Summary of trauma patient characteristics.

Legend for table S2

Table S3. Closeness of trauma patient factor concentrations to values from control mean plasma.

Table S4. Closeness of trauma patient factor concentrations to means from 20 normal plasma samples.

Table S5. Unsuccessful k-means classification of normal and trauma using four CAT dimensions.

Table S6. Unsuccessful k-means classification of normal and trauma using seven concentrations, equivalent to using the first two and the first three principal components.

Table S7. Conversion factors used for Hockin-Mann model prediction of trauma CATs.

Legends for tables S8 and S9

Table S10. Mean of the SD of nonspiked factor concentrations across multiple normal plasma samples.

Table S11. Maximum nonspiked factor concentration in normal plasma samples.

Legends for tables S12 and S13

References (18–21)

Other Supplementary Material for this manuscript includes the following:

(available at www.sciencetranslationalmedicine.org/cgi/content/full/9/371/eaaf5045/DC1)

Table S2. Normal and trauma patient plasma sample data (provided as an Excel file).

Table S8. Thrombin dynamical system linearity testing data (provided as an Excel file).

Table S9. Factor addition independence testing data (provided as an Excel file).

Table S12. Factor perturbation data (provided as an Excel file).

Table S13. Ancillary factor perturbation data and model validation data (provided as an Excel file).

Supplementary Materials and Methods

Measured CAT thrombin trajectory data are in units of nM. The time data are in minutes. The measured concentrations of blood protein factors II, V, VII, VIII, IX, X, and ATIII in each normal and trauma sample are expressed as a percentage of the mean concentrations in normal plasma. The INR reference range is 0.9 to 1.3. The PTT reference range is 28.0 seconds to 40.0 seconds. The PT reference range is 11.6 seconds to 15.8 seconds.

Computational approaches on calibrated automated thrombogram data and model-free machine learning techniques applied to factor concentration measurements

From a patient's measured CAT thrombin trajectory data, it is possible to extract parameters such as peak thrombin concentration P , peak concentration time T_p , delay T (by determining the intersection between the trajectory and the perpendicular to a tangent of the rising CAT half-peak, with the perpendicular also intersecting the time-intercept of that tangent), rise time $T_p - T$, and area under the CAT curve IIa_{tot} . Fig. 2C indicates that the CAT trajectories of trauma patients tend to have a shorter time-delay T , a faster thrombin burst, a faster thrombin decay, and more pointed trajectory peaks than normal CAT trajectories. Accordingly, we tested the possibility of separating CAT trajectories into the two patient classes via k-means clustering by using a four-dimensional space, with the dimensions being T , the upslope of a CAT trajectory defined by $\frac{P}{(T_p - T)}$, the downslope of a CAT trajectory (under the assumption of a triangular shape) defined by $\frac{P}{\frac{2IIa_{tot}}{P} - (T_p - T)}$, and the sampled second derivative of the CAT trajectory at time T_p .

Model-free machine learning techniques for differentiating trauma patient plasma from normal plasma based only upon initial concentrations of protein factors II, V, VII, VIII, IX, X, and ATIII consisted of:

1. K-means clustering of the 60 total normal and patient samples according to the seven concentrations.
2. A principal component analysis with centering on all 60 samples followed by
 - a. k-means clustering of the representation of the 60 samples in the principal component space using either the first two dominant components or the first three dominant components.
 - b. support vector machines application to determine a non-linear curve in the space of the two dominant components that separates trauma patients from normal.

The two dominant components of variance can be used in lieu of the measured initial concentrations of protein factors II, V, VII, VIII, IX, X, and ATIII in each patient blood sample for plotting together with patient demographics and outcomes to obtain three-dimensional visual depictions of each sample.

Our implementation of the popular Hockin-Mann model (*11*) was validated with the results in (*11*) and checked for correctness by ensuring the equivalence of our implementation's outputs with those produced by another implementation independently developed by colleagues at the University of California, Santa Barbara. To produce the simulation results that are summarized in Fig. 2E, our implementation of the Hockin-Mann model required initial concentrations for protein factors II, V, VII, VIII, IX, X, and ATIII to be in units of molarity, M, necessitating a units conversion of the values in table S2. The conversion factors that we used are listed in the fourth column of table S7. These conversion factors resulted from dividing the initial concentrations used in (*11*) for mean plasma (the third column of table S7) by the factor concentration percentage measurements of control mean plasma (the second column of table S7).

Linear time-invariant approximation of the calibrated automated thrombogram for a standardized measurement input value

There is a theoretical and modeling convenience to the current experimental practice of using 5 pM tissue factor concentration as a CAT input, which is suggested by an output trajectory's shape. The CAT trajectories generated from various initial tissue factor concentrations yield insight into the linearity (or lack thereof) of the underlying thrombin dynamical system. A linear dynamical system is one where, for any two inputs $u(t)$ and $v(t)$ that respectively generate outputs $y(t)$ and $z(t)$, the provision of a scaled input results in a

similar scaling of the original output (for example, a $5u(t)$ input produces a $5y(t)$ output), and the provision of an input that is the sum of two other inputs results in an output that is itself the sum of the outputs that would individually result from each input [for example, an input of $5u(t)+v(t)$ generates an output that is $5y(t)+z(t)$]. A nonlinear dynamical system is a dynamical system for which the definition of linearity is not satisfied. The advantages of linear dynamical systems include their description by relatively simple models that have a rich and well-developed analytical theory and their broad applicability wherever linearity holds, which imply that responses to a small set of inputs can be used for general output characterization and prediction in a larger region of the input space. The measured CAT trajectories in Fig. 2C produced by the thrombin dynamical system are also time-invariant: applying the typical 5 pM tissue factor concentration input after a delay d [in other words, providing $u(t-d)$] generates a CAT trajectory that is identical to the one generated from the application of the original input $u(t)$, except that the output trajectory is additionally shifted in time by d [in other words, $y(t-d)$ is obtained instead of $y(t)$].

Fig. S6A illustrates sample CAT trajectories that could be produced by an underlying thrombin dynamical system that is linear and time-invariant, using one possible model [for a system having thrombin concentration time-history as a single output $y(t)$ and tissue factor concentration time-history as a single input $u(t)$] that is developed and analyzed in this work. The computed trajectories in fig. S6A show that the peak thrombin concentration P scales correspondingly with increases in tissue factor concentration, whereas the delay T , the peak concentration time T_p , and the rise time $T_p - T$ all stay constant. Real data in fig. S6B show that the underlying thrombin dynamical system is nonlinear, because the experimental CAT behavior does not match fig. S6A when given scaled initial tissue factor concentration inputs of 1 pM, 5 pM, 10 pM, 15 pM, and 20 pM (although the system is still time-invariant as explained above). Specifically, for the 20 normal plasma samples in our dataset and a pool of different non-injured plasma samples, the P and the $T_p - T$ dependence on input tissue factor concentration (fig. S6C and D, respectively) is affine (linear plus a constant), the T dependence on the input (fig. S6E) is described by a power law, and the area under the CAT curve (fig. S6F) is twice the product of P and $T_p - T$. Nevertheless, a linear function without an offset can closely approximate P (fig. S6C), a constant-value fit of $T_p - T$ and of T is a good approximation of an output caused by

inputs within a neighborhood of 5 pM of initial tissue factor concentration (fig. S6D,E), and twice the product of the no-offset P fit and the constant value $T_p - T$ fit is still an adequate (within nearly one standard deviation) approximation of the Πa_{tot} that is generated by inputs near 5 pM of initial tissue factor concentration. Thus, it is possible to approximate the thrombin dynamical system as a linear time-invariant one for inputs of about 5 pM of initial tissue factor concentration, which is the typical value.

The implication of the approximated system linearity is that a relatively simple dynamical system model exists that takes tissue factor concentration input $u(t)$ to generate thrombin concentration output $y(t)$ when $u(t) \approx 5$ pM, which is in direct contrast with the more involved and nonlinear current trauma coagulation modeling approaches [such as (11) and (14)]. In this study, a linear dynamical system model of trauma coagulation at a fixed input tissue factor concentration of 5 pM is produced, and it includes the ascertained dynamic effects of different blood protein factor concentrations. In particular, because it is possible to quickly (within a few minutes) measure the concentration of protein factors II, V, VII, VIII, IX, X, and ATIII in a blood sample that is taken from a trauma patient upon hospital admittance, it is desirable for a CAT model to use the concentrations of these seven factors. Incorporation of the role played by these factors in the model will facilitate the delivery of personalized concentrations that aim to correct a trauma patient's predicted CAT by changing the clotting dynamics. Such delivery, which constitutes open-loop regulation of thrombin, differs from control via tissue factor, a process that necessitates concentration inputs where the system linearity approximation we use is not always valid.

Model development methodology

Model determination: identifying a thrombin dynamical system model

Exponential functions are an important component of linear dynamical systems. It is possible to empirically approximate a CAT peak with a function that multiplies a positive power of time and a decaying time exponential (two examples are presented in fig. S6G). Suppose that the following non-delayed function approximates thrombin concentration: $y(t) = \beta t^2 e^{-\alpha t}$, where α and β are constants. This approximation will be justified shortly with traditional system identification and parameter-quantity minimization techniques. In the frequency domain, the dynamical system output becomes

$$Y(s) = \frac{2\beta}{(s + \alpha)^3} = \frac{2\beta}{s^3 + 3\alpha s^2 + 3\alpha^2 s + \alpha^3} \quad [4]$$

after applying the Laplace transform to $y(t)$.

The tissue factor that initiates coagulation in a blood sample until its quick depletion at CAT start may be considered an impulse input that is applied to the thrombin dynamical system. Thus, $y(t)$ and $Y(s)$ are equivalent to the impulse response of the system in the time and frequency domains, respectively, that is caused by the respective impulse input $u(t)$ or $U(s)$ (for example, a 5 pM impulse at $t=0$ min). For the unit impulse $U(s)=1$, the corresponding thrombin transfer function from $U(s)$ to $Y(s)$, $Y(s)/U(s)$, is the right side of [4].

Hence, a transfer function model from tissue factor concentration [pM] to thrombin concentration [μ M] with time-delay T that is generalized to improve upon the depicted fit of $y(t) = \beta t^2 e^{-\alpha t}$ in fig. S6G is

$$\frac{Y(s)}{U(s)} = \frac{b}{s^3 + a_2 s^2 + a_1 s + a_0} e^{-sT}. \quad [5]$$

Five parameters have to be identified: a_2 , a_1 , a_0 , b , and T . The transfer function without time-delay in [5] is strictly proper, and the degree of the denominator of this transfer function without time-delay (the degree of the “characteristic polynomial,” which is three) indicates that a differential equation representation of the system has three states. If a function of form $y(t) = \beta t e^{-\alpha t}$ (fig. S6G) is chosen as the first approximation instead of $y(t) = \beta t^2 e^{-\alpha t}$, the associated characteristic polynomial is second degree, which indicates a two-state differential equation system, and the transfer function with time-delay requires the identification of four parameters. Traditional system identification (18) techniques (for example, discrete-time autoregressive exogenous input, ARX, deployed with Matlab’s built-in functionality) applied to sampled CAT data demonstrate that a three-state model with a single numerator constant term satisfies the Akaike information criterion (AIC) (19), a two-state model with a single numerator constant term satisfies Rissanen’s minimum description length (MDL) principle (20), and models with four or more states overfit the data. Here, AIC and MDL are different criteria for upper-bounding the degree of the characteristic polynomial and the number of numerator terms, while still ensuring model suitability through a minimization of output (fit) variance. Thus, models with more states than the number that satisfies a criterion will overfit (according to that

criterion's interpretation) the applied data, and models with fewer states than the number that satisfies a criterion will be incomplete (according to that criterion's interpretation), with greater unexplained output variance. Because we are not concerned with order size due to our model's simplicity, we used the AIC criterion to choose between the models, selecting the order-three system in [5]. The five parameters of [5] may be determined for each of the 20 normal and 40 patient CATs with a near-perfect nonlinear least-squares fit (fig. S6G) of the system's impulse response using Matlab Simulink and the trust-region-reflective algorithm of the Simulink design optimization (SDO) toolbox.

Model determination: alternate thrombin dynamical system modeling method

One possibility out of infinitely many for the linear time-invariant differential equation dynamics that yield [5] after the application of the Laplace transform is the following state-space realization (21):

$$\begin{aligned}
 \dot{x}_1(t) &= -a_2 x_1(t) + x_2(t), \\
 \dot{x}_2(t) &= -a_1 x_1(t) + x_3(t), \\
 \dot{x}_3(t) &= -a_0 x_1(t) + b v(t), \\
 y(t) &= x_1(t),
 \end{aligned}
 \tag{6}$$

which is the canonical “completely observable” realization that ensures that all three states $x_1(t)$, $x_2(t)$, and $x_3(t)$ affect the observed output $y(t)$, with realized system input $v(t)$. This $v(t)$ is the time-delayed input $u(t - T)$, since the tissue factor effect in fig. S6E puts T at the input.

To interpret [6], consider the activation or inhibition of the protein factors in Fig. 1A and the reactions directly affecting or affected by these factors. First, because $y(t)$ is thrombin concentration, the output equation $y(t) = x_1(t)$ of [6] implies that $x_1(t)$ represents the time-history of thrombin concentration. Because the first differential equation of [6] shows in part that thrombin inhibits its own production at a rate a_2 , there is agreement with thrombin's known roles in the production of inhibitory APC and reaction with inhibitory ATIII. This differential equation also indicates that the concentration of thrombin grows proportionally with $x_2(t)$, suggesting that the protein factor whose concentration time-history is represented by $x_2(t)$ is either Xa or the Xa-Va complex. Next, the input appears in the third differential equation of [6]. Thus, candidates for $x_3(t)$ are the concentration time-histories of tissue factor, the tissue factor-

VII complex, and the tissue factor-VIIa complex. These protein factors are depleted as more thrombin is produced, in accordance with the first part of this differential equation. Because the second differential equation of [6] relates the increase of $x_2(t)$ proportionally with $x_3(t)$, both candidates for $x_2(t)$ narrow $x_3(t)$ to the concentration time-history of the tissue factor-VIIa complex. Also, because $b = Ka_0$, which implies that $\dot{x}_3(t) = a_0(Kv(t) - x_1(t))$, the concentration of the tissue factor-VIIa complex can be thought of as being driven by the “error” between a scaling of the input tissue factor concentration and thrombin concentration, at rate a_0 . Lastly, the second differential equation suggests that thrombin inhibits $x_2(t)$ at rate a_1 , and $x_2(t)$ must therefore represent the concentration time-history of the Xa-Va complex.

Hence, the dynamical model states of a completely observable realization may be related to the concentrations of thrombin, the Xa-Va complex, and the tissue factor-VIIa complex, with an input of tissue factor concentration and an output of thrombin concentration. Biologically, this model’s states correspond to the chief participants of the thrombin generation process. A simplified schematic of the known coagulation process in line with this model is provided in Fig. 1B. Although the concentrations of the Xa-Va and tissue factor-VIIa complexes cannot be measured, the use of this model provides clinicians with computed dynamical estimates of the concentration behavior of these complexes upon clotting stimulation. Should these complexes become measurable, the ensuing measurements can help validate the model interpretation of this section.

Model determination: implications of the control-theoretic parameters on tuning the thrombin dynamical system

The control-theoretic parameters p , ω_n , and T serve as k-means classifiers, rendering four distinct clusters when chosen by adjusted figure of merit scoring (fig. S8). The control-theoretic parameters provide insight into the underlying dynamics. Although the equivalent temporal parameters a_2 , a_1 , a_0 , and b capture the known thrombin generation process (see above), the main text explains why the control-theoretic parameter representation of coagulation dynamics is better suited for modeling the effects of protein factor concentrations when compared to temporal parameters. Fig. S8 will thus ultimately represent visual insight into how coagulation dynamics could be changed, and hence, control-theoretic parameter controllability:

the feasibility of moving parameters and the range of locations that are reachable from the starting points visualized there. Increasing any one factor concentration affects all control-theoretic parameters together during tests of factors II, VIII, and X (see below and figs. S10-S13), and by determining the parameter effects induced by the untested concentrations of factors V, VII, IX, and ATIII, it should be possible to ascertain the full range of feasible movement within the control-theoretic parameter space given an initial condition and to determine which factor concentrations need to be increased and by how much.

Model construction and parameter estimation: tuning the thrombin dynamical system

Measurements of the concentration of blood protein factors in normal plasma samples after an additional concentration of a single factor was spiked in (table S9) were collected to determine interdependence of factor concentrations, which would be revealed if other concentrations also increased or decreased simultaneously with the perturbed factor concentration. For each plasma sample that was spiked with various concentrations of a single factor, the standard deviation of the non-spiked factor concentrations was calculated. If the standard deviation of a non-spiked factor concentration were large, this would indicate a coordinated movement of that factor concentration with the spiked factor. Summary (mean) statistics for the standard deviation of non-spiked factor concentrations are presented in table S10 and Fig. 3D. The latter table normalizes the data in the former table according to the normalization factors in table S11, which represent the maximum measured non-spiked concentration values in the normal plasma samples. Because the normalization factors used here are taken from normal plasma samples and are often less than the observed maximum factor concentrations in trauma plasma samples, we expect that the use of the latter would further diminish the values in Fig. 3D.

Supplementary Figures

MODEL PRELIMINARIES	MODEL DETERMINATION	MODEL CONSTRUCTION	MODEL PREDICTION
<ul style="list-style-type: none"> Find an assay (the CAT) to measure the coagulation dynamical system's thrombin concentration output in a way that is conducive to control-theoretic analysis, and find blood protein factors that affect the dynamical system and whose concentrations are rapidly measurable (factors II, V, VII, VIII, IX, X, and ATIII). Determine the applicability of a particular instance of dynamical systems theory, which is when the considered dynamical systems are linear, so that the development of a relatively simple model form with a rich analytical foundation can be facilitated. Show that this linear approximation is valid at the typical CAT operating point of 5 pM of tissue factor concentration input. 	<ul style="list-style-type: none"> To ascertain a phenomenological model of the trauma coagulation process, first identify a linear dynamical system model structure in the frequency domain whose output response matches the form of the CAT output for the same type of system impulse input. Determine the model's order, using AIC, MDL, and the quality of fits to measured CAT output data. Analyze the fits to obtain insights into model form: here, that a two-subsystem composition having traditional control-theoretic parameters exists, and that the model form is applicable no matter the patient or type/presence of injury, with any observed parametric differences caused by differences in factor concentration. Interpret the model in the time domain and show that there is compatibility with existing knowledge of the coagulation cascade. 	<ul style="list-style-type: none"> Experimentally show how CAT output changes with factor concentration perturbations, how the changes are linear, and how these changes can be recapitulated with the control-theoretic parameters. This constructs a map between factor concentrations and control-theoretic parameters. Because the effects of perturbations are linear, use forward stepwise linear regression to infer the requisite map while imposing observed experimental relationships. 	<ul style="list-style-type: none"> Verify that the developed model is able to accurately recapture the CAT trajectories of patients with different types of injuries. Cross-validate this verification (using five-fold cross-validation for inference mapping). Experimentally validate (for both normal and trauma patient blood samples) that the developed model can predict a CAT when given non-dataset factor concentrations, which then also serves as a means of open-loop control.



Fig. S1. Summary of our model development process.

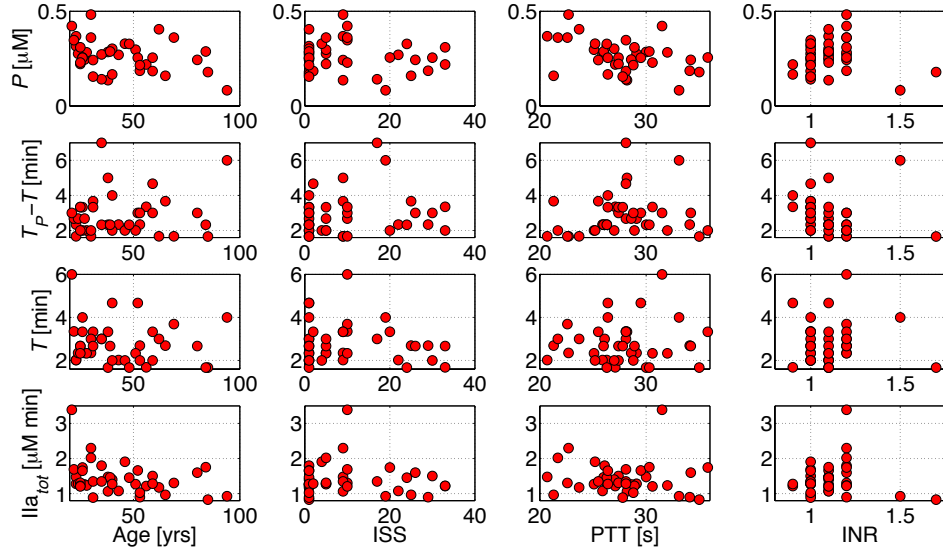


Fig. S2. Lack of correlation between trauma patient characteristics and outcomes. The clinical characteristics that we evaluated were age, ISS, PTT, and INR, and the outcomes were CAT parameters peak thrombin concentration P , rise time $T_p - T$ (where T_p is the time of the peak and T is a time-delay that precedes the initiation of the thrombin concentration peak response), delay T , and the total thrombin produced during clotting, $I\text{Ia}_{tot}$. The first row shows that P is not correlated with age (first column, $R^2 = 0.11$), ISS (second column, $R^2 = 0.02$), PTT (third column, $R^2 = 0.16$), and INR (fourth column, $R^2 = 0.00$), in that order. Similarly, the second row shows that $T_p - T$ is not correlated with age ($R^2 = 0.02$), ISS ($R^2 = 0.02$), PTT ($R^2 = 0.03$), and INR ($R^2 = 0.03$), the third row shows that T is not correlated with age ($R^2 = 0.01$), ISS ($R^2 = 0.03$), PTT ($R^2 = 0.01$), and INR ($R^2 = 0.00$), and the fourth row shows that $I\text{Ia}_{tot}$ is not correlated with age ($R^2 = 0.10$), ISS ($R^2 = 0.01$), PTT ($R^2 = 0.01$), and INR ($R^2 = 0.00$).

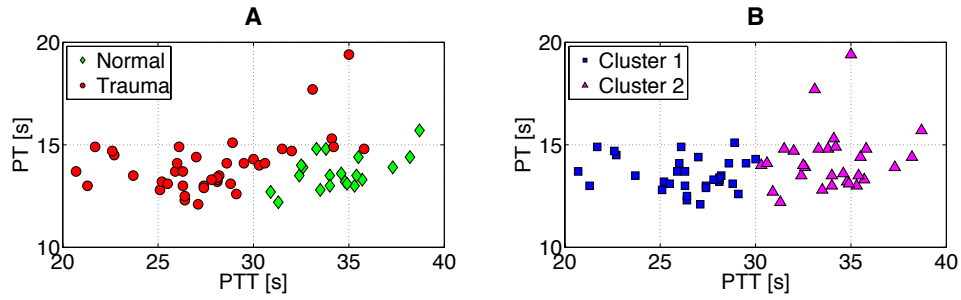


Fig. S3. Overlap of normal and trauma patient classes. (A) Normal and trauma patient classes overlap in a space of PT and PTT, which makes classification, for instance via k-means clustering in (B), problematic: although cluster 1 (blue) contains trauma patients only, cluster 2 (magenta) includes both trauma and normal patients.

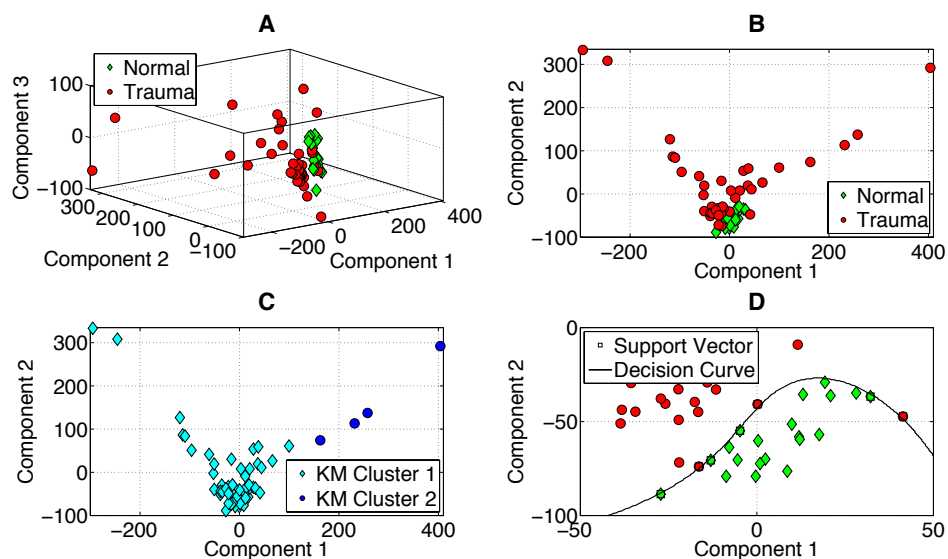


Fig. S4. Model-free machine learning techniques applied to measured factor concentrations. After a principal component analysis (PCA) with centering, the seven initial concentrations of protein factors II, V, VII, VIII, IX, X and ATIII in 20 normal and 40 trauma patient plasma samples have a primary principal component that explains 47.1% of total variance, a secondary principal component that explains 41.5% of total variance, and a tertiary principal component that explains 7.7% of total variance. These three component dimensions are plotted in (A), and only the first two are plotted in (B). In (C), two-cluster classification with k-means is unable to recover the correct normal and trauma classification. (D) The machine learning technique called support vector machines can determine a non-linear curve in the space of the two dominant components that cleanly separates trauma patients from normal; this curve relies on support from three trauma patient vectors and four normal vectors. However, the separation is minimal, and work still remains on assigning meaning to the mapping from factor concentration space to principal component space, so that the effects of changes in factor concentrations on principal components can be known in advance, along with how to move trauma patients in the principal component space by factor addition.

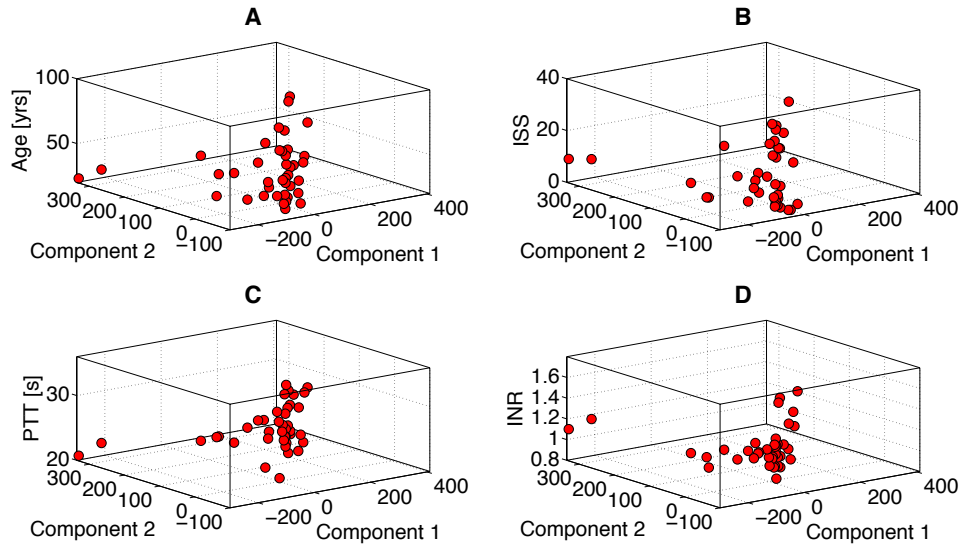


Fig. S5. Lack of correlation between trauma patient characteristics and principal components. Trauma patient characteristics grouped by age (A), ISS (B), PTT (C), and INR (D) are not correlated with the two principal components that explain most of the variance in the measured concentrations of protein factors II, V, VII, VIII, IX, X and ATIII in each patient blood sample ($R^2 = 0.06$, $R^2 = 0.01$, $R^2 = 0.30$, and $R^2 = 0.03$, respectively).

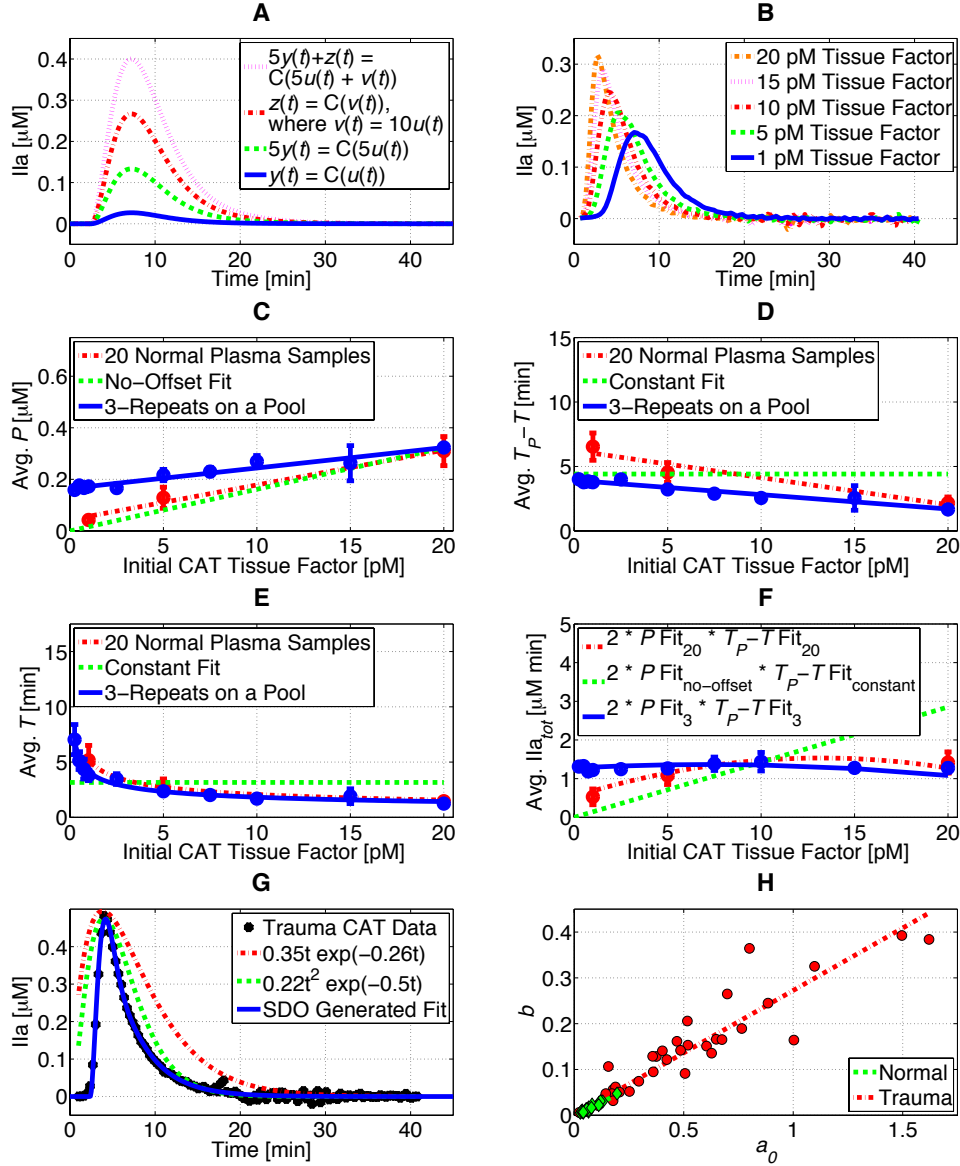


Fig. S6. Linearity, justification, and fit of a thrombin dynamical system model. (A) Sample CAT trajectories produced by one possible linear time-invariant representation of the underlying thrombin dynamical system that is developed and analyzed in this work. For any inputs $u(t)$ and $v(t)$ to the clotting system C that produce outputs $y(t) = C(u(t))$ and $z(t) = C(v(t))$, respectively, the clotting system C is linear if $C(\alpha u(t) + \beta v(t)) = \alpha C(u(t)) + \beta C(v(t))$, and it is time-invariant if $y(t-d) = C(u(t-d))$. The inputs chosen here demonstrate the effects of the series $1u(t)$, $5u(t)$, $10u(t)$, and $15u(t)$, and show that P is scaled but that T and T_p are unchanged. (B) Despite time-invariance, the experimental CAT trajectories generated by initial tissue factor concentration inputs of 1 pM, 5 pM, 10 pM, 15 pM, and 20 pM applied to a pool of

normal plasma samples do not match the depicted (A) linear behavior. (C) Although P behavior is affine (linear plus an offset) (red biological replicates $R^2 = 0.99$, blue technical replicates $R^2 = 0.94$), it can be closely approximated by a linear function without an offset to obtain (A) scaling behavior. (D) The rise time $T_p - T$ is also an affine function of the input (red biological replicates $R^2 = 0.93$, blue technical replicates $R^2 = 0.94$), but a constant-value fit of the data as required by (A) is a good approximation in the vicinity of a standardized 5 pM input. Although such an approximation to obtain a linear dynamical system model precludes varying tissue factor concentration as a control actuator, such control is not tackled in this paper. (E) The delay T (which was extracted from each CAT trajectory by determining the intersection between that trajectory and the perpendicular to a tangent of the rising CAT half-peak, with the perpendicular also intersecting the time-intercept of that tangent) is affected by initial tissue factor concentration via a power law (red biological replicates $R^2 = 1.00$, blue technical replicates $R^2 = 0.98$). A constant-value fit of the data as required by (A) is also a good approximation in the vicinity of the aforementioned 5 pM standardized input. (F) Ia_{tot} is twice the product of P and $T_p - T$, and is adequately captured (within nearly one standard deviation) around the standardized 5 pM input by a linear system assumption that uses the approximations of (C) and (D). (C)-(F) Error bars indicate the standard deviation. (G) A sample trauma CAT, which can be approximated by exponential functions that are an important component of linear dynamical systems, is approximated here by a function that is the product of time and a decaying time exponential as well as the product of squared time and a decaying time exponential. When the latter also includes a delay, it is possible to tune the function to fit the measured thrombin concentration data almost perfectly ($R^2 = 1.00$ for this sample). (H) Fitted b parameters of all CATs are linearly related to their corresponding fitted a_0 parameters; the parameters are marked without a line, whereas the least-squares linear relation is depicted as a line without any markers. The linear relation for the normal fitted CAT parameters overlies the linear relation for the trauma fitted CAT parameters almost exactly ($R^2 = 0.93$ for normal CATs, $R^2 = 0.86$ for patient CATs).

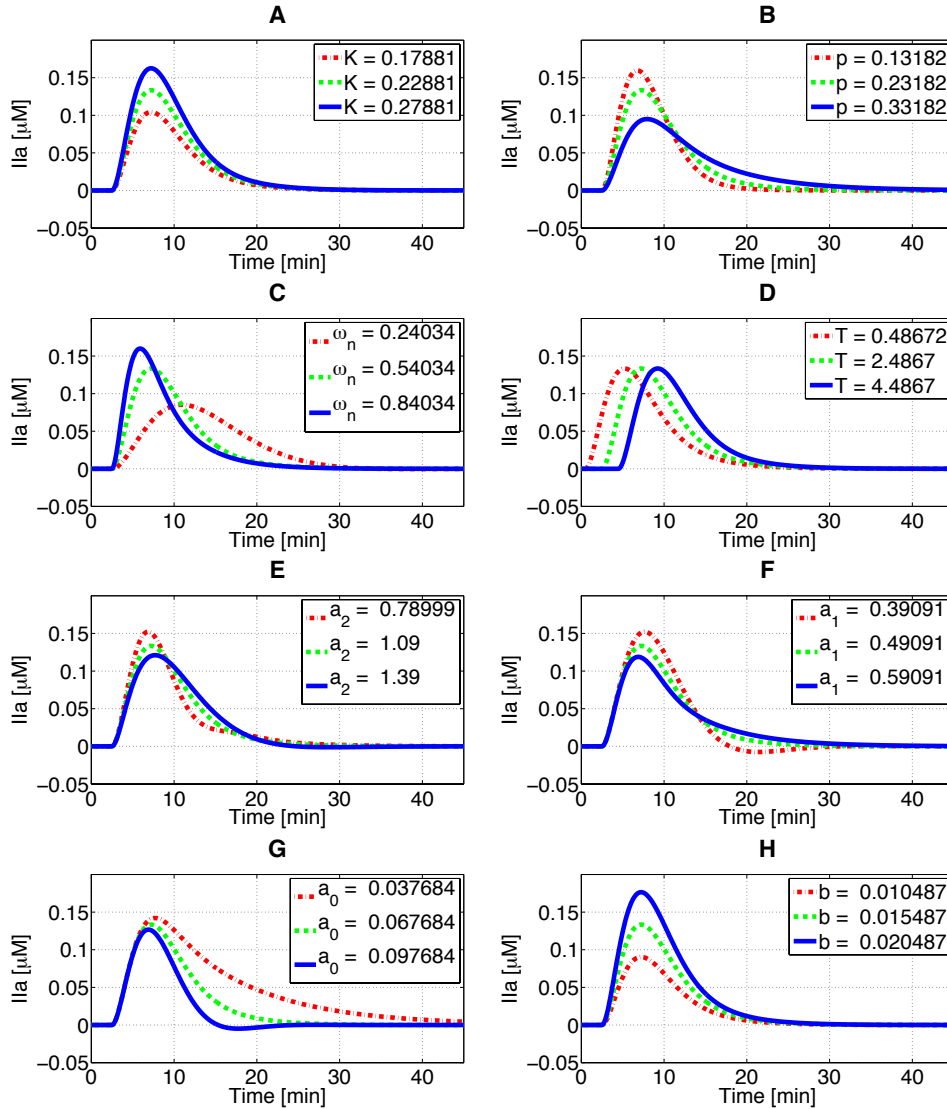


Fig. S7. Model control-theoretic and temporal parameter effects. (A)-(D) The effect of changes in model control-theoretic parameters on a reference average normal $y(t)$, plotted with a green dashed line. (A) K scales $y(t)$. (B) p primarily affects the overshoot of $y(t)$. (C) ω_n primarily affects the rise time and settling time of $y(t)$. (D) T shifts $y(t)$ in time. (E)-(H) The effect of changes in model temporal parameters on a reference average normal $y(t)$, plotted with a green dashed line. (E) shows that a_2 , (F) shows that a_1 , and (G) shows that a_0 each affect $y(t)$ overshoot, settling time and secondary oscillations. (H) b scales $y(t)$.

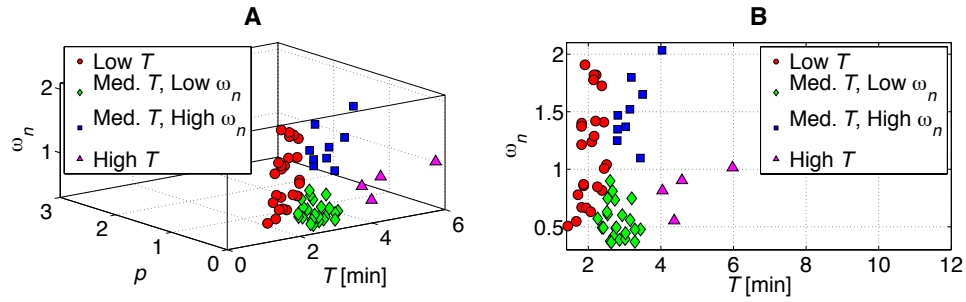


Fig. S8. K-means classification using control-theoretic parameters. (A) Control-theoretic parameters p , ω_n , and T as k-means classifiers for four clusters. (B) Projection in the ω_n - T plane. Most normal plasma samples belong to the medium delay, low natural frequency cluster. Like the CAT parameters in Fig. 2D, the control-theoretic parameters do not distinguish between normal and patient CATs.

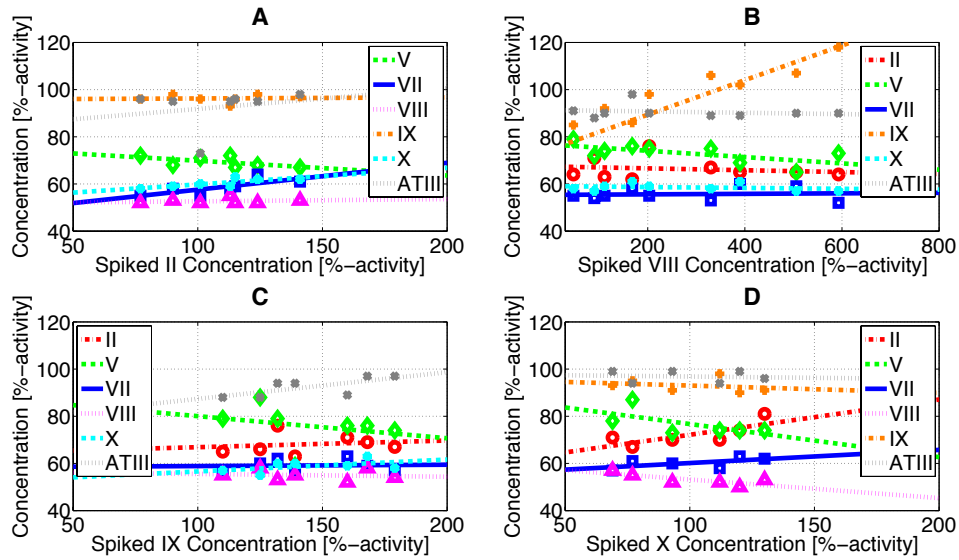


Fig. S9. Independence of factor addition to normal plasma. In (A), (B), (C), and (D), spiking factors II, VIII, IX, and X, respectively, into normal plasma sample #14492 does not substantially change the concentrations of the other non-spiked factors. Trend lines are included as a visual aid. Results for additional normal plasma samples are available in table S9. These experimental results disprove a seemingly coordinated increase in factor IX concentration with that of factor VIII in (B); see also tables S10 and S11.

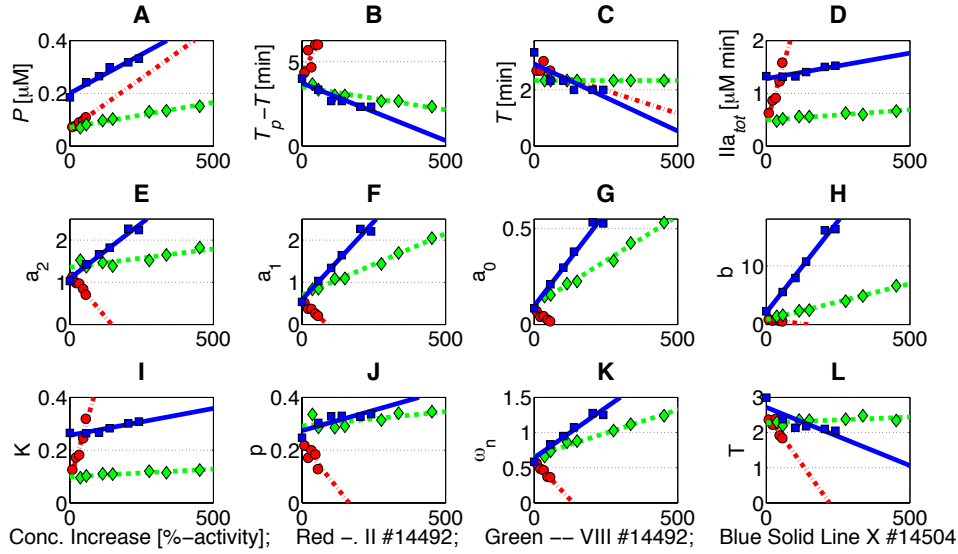


Fig. S10. Parameter effects caused by increasing the concentration of factor II, VIII, or X in a sample of normal plasma. (A) Effect on peak thrombin concentration, red $R^2 = 0.98$, green $R^2 = 0.97$, blue $R^2 = 0.95$. (B) Effect on rise time, red $R^2 = 0.58$, green $R^2 = 0.89$, blue $R^2 = 0.87$. (C) Effect on delay, red decreasing, green no effect, blue $R^2 = 0.70$. The delay shown here was extracted (just as in fig. S6E) from each measured CAT trajectory by determining the intersection between that trajectory and the perpendicular to a tangent of the rising CAT half-peak, with the perpendicular also intersecting the time-intercept of that tangent. (D) Effect on total thrombin produced, red $R^2 = 0.93$, green no effect, blue no effect. (E) Effect on a_2 , red $R^2 = 0.95$, green $R^2 = 0.72$, blue $R^2 = 0.97$. (F) Effect on a_1 , red $R^2 = 0.95$, green $R^2 = 0.99$, blue $R^2 = 0.97$. (G) Effect on a_0 , red $R^2 = 0.90$, green $R^2 = 0.99$, blue $R^2 = 0.98$. (H) Effect on b , red $R^2 = 0.79$, green $R^2 = 0.99$, blue $R^2 = 0.98$. (E)-(H) The trend lines for factor II also provide insight into why it is not possible to add much of this factor; increases in factor II cause all temporal parameters to decrease, but because these parameters are lower-bounded by 0, it is not possible to surpass this constraint. Here, a_0 is the temporal parameter that first encounters the constraint. (I) Effect on gain, red $R^2 = 0.93$, green no effect, blue no effect. (J) Effect on cut-off frequency, red $R^2 = 0.58$, green increasing, blue $R^2 = 0.68$. (K) Effect on natural frequency, red $R^2 = 0.96$, green $R^2 = 0.98$, blue $R^2 = 0.95$. (L) Effect on SDO-fitted delay, red $R^2 = 0.73$, green no effect, blue $R^2 = 0.71$. The delay trends here are consistent with that shown in C.

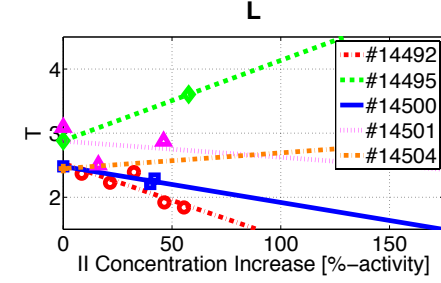
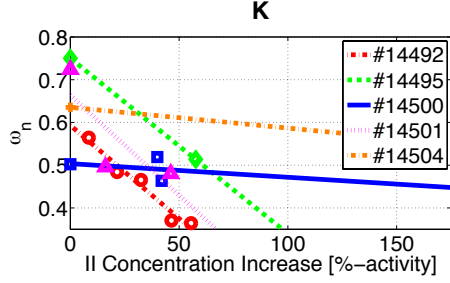
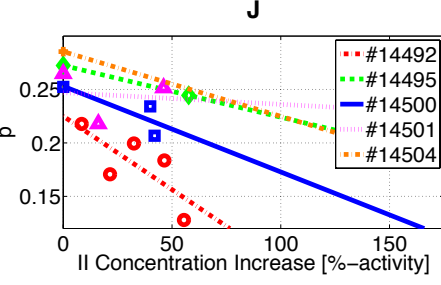
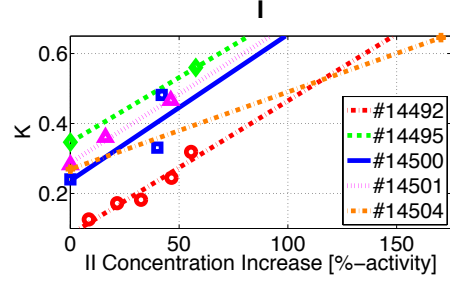
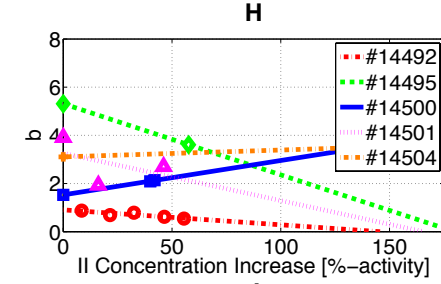
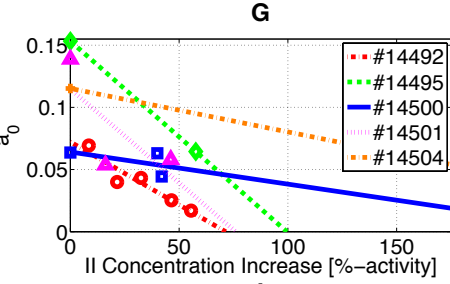
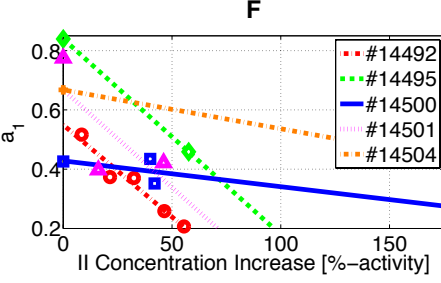
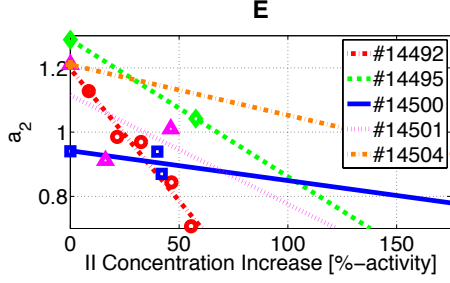
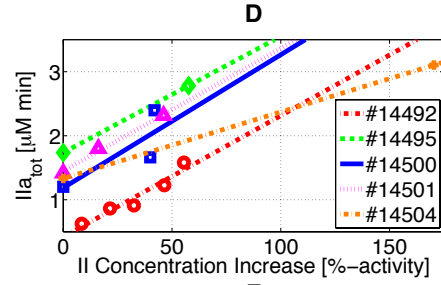
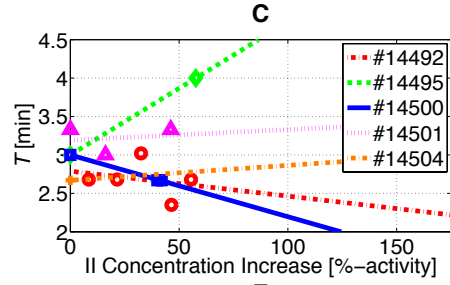
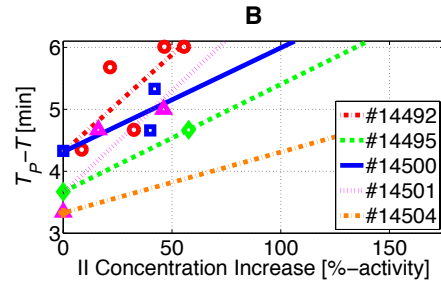
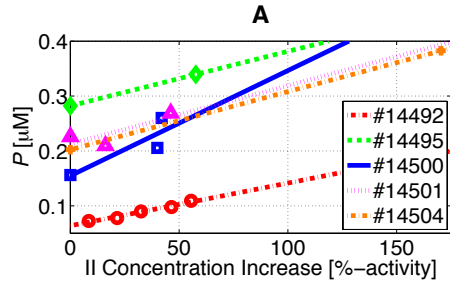


Fig. S11. Parameter effects caused by increasing the concentration of factor II in five normal plasma samples. In five normal plasma samples, an increase in the concentration of factor II increases the CAT trajectory peak thrombin concentration P (A), increases the rise time $T_p - T$ (B), decreases the delay T (C), and increases the total thrombin produced Πa_{tot} (D). A concentration increase of factor II decreases temporal parameters a_2 , a_1 , a_0 , and b in (E), (F), (G), and (H), respectively. An increase in the concentration of factor II increases the gain K (I) and decreases the cut-off frequency p (J), the natural frequency ω_n (K), and the SDO-fitted delay T (L) [see also (C); additionally, inference results with the complete dataset confirm this conclusion].

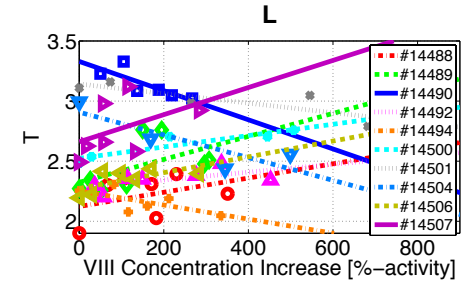
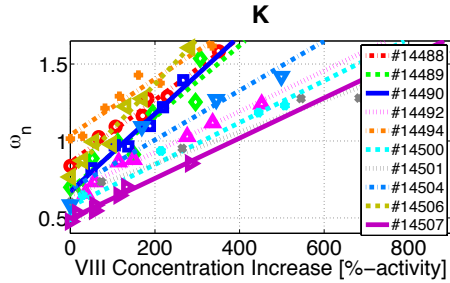
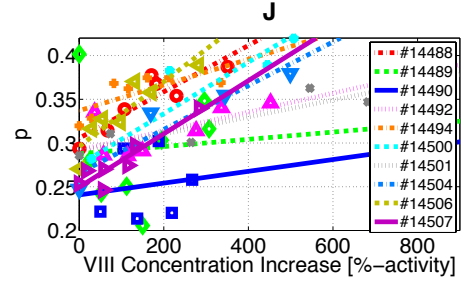
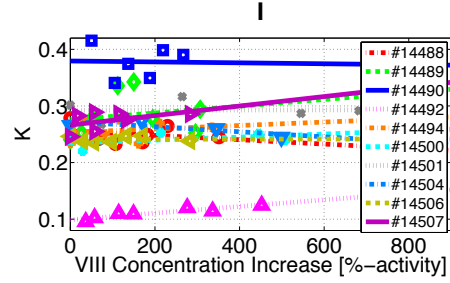
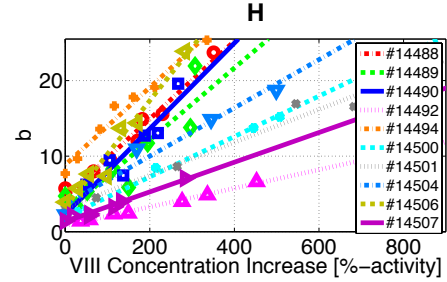
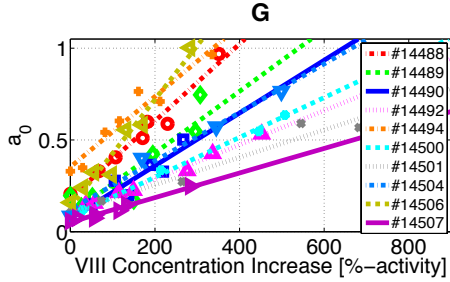
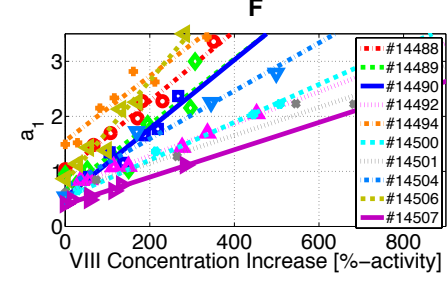
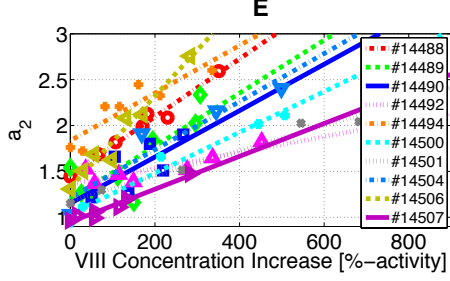
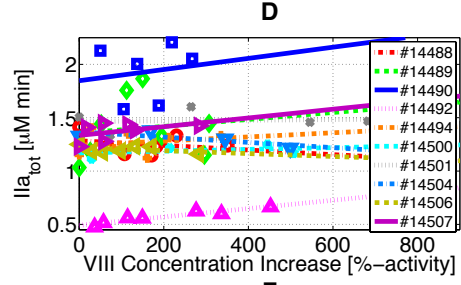
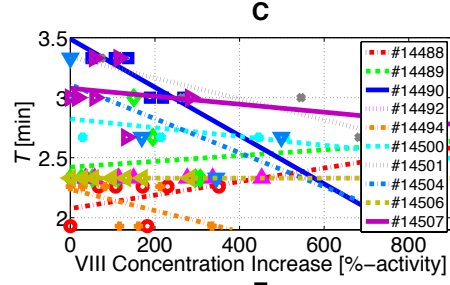
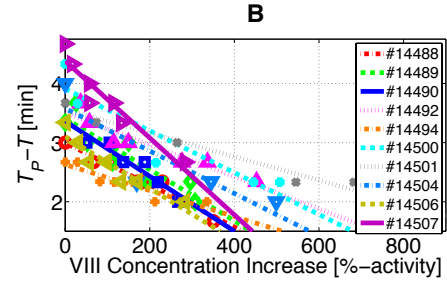
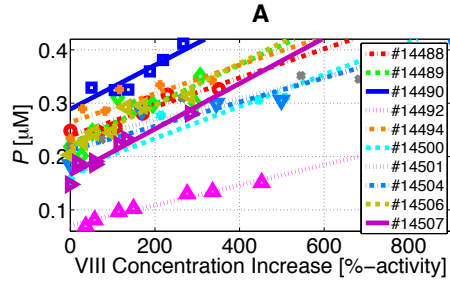


Fig. S12. Parameter effects caused by increasing the concentration of factor VIII in 10 normal plasma samples. In ten normal plasma samples, a concentration increase of factor VIII increases CAT peak thrombin concentration P (**A**) and decreases the rise time $T_p - T$ (**B**). The delay T (**C**) and the total thrombin produced Πa_{tot} (**D**) are unaffected. A concentration increase of factor VIII increases temporal parameters a_2 (avg. $R^2 = 0.84$), a_1 (avg. $R^2 = 0.95$), a_0 (avg. $R^2 = 0.94$), and b (avg. $R^2 = 0.95$) in (**E**), (**F**), (**G**), and (**H**), respectively. An increase in factor VIII concentration does not affect the gain K (**I**). However, the cut-off frequency p (avg. $R^2 = 0.79$ in 7 samples with a trend) (**J**) and the natural frequency ω_n (avg. $R^2 = 0.95$) (**K**) increase. An increase in factor VIII concentration does not conclusively affect the SDO-fitted delay T (**L**).

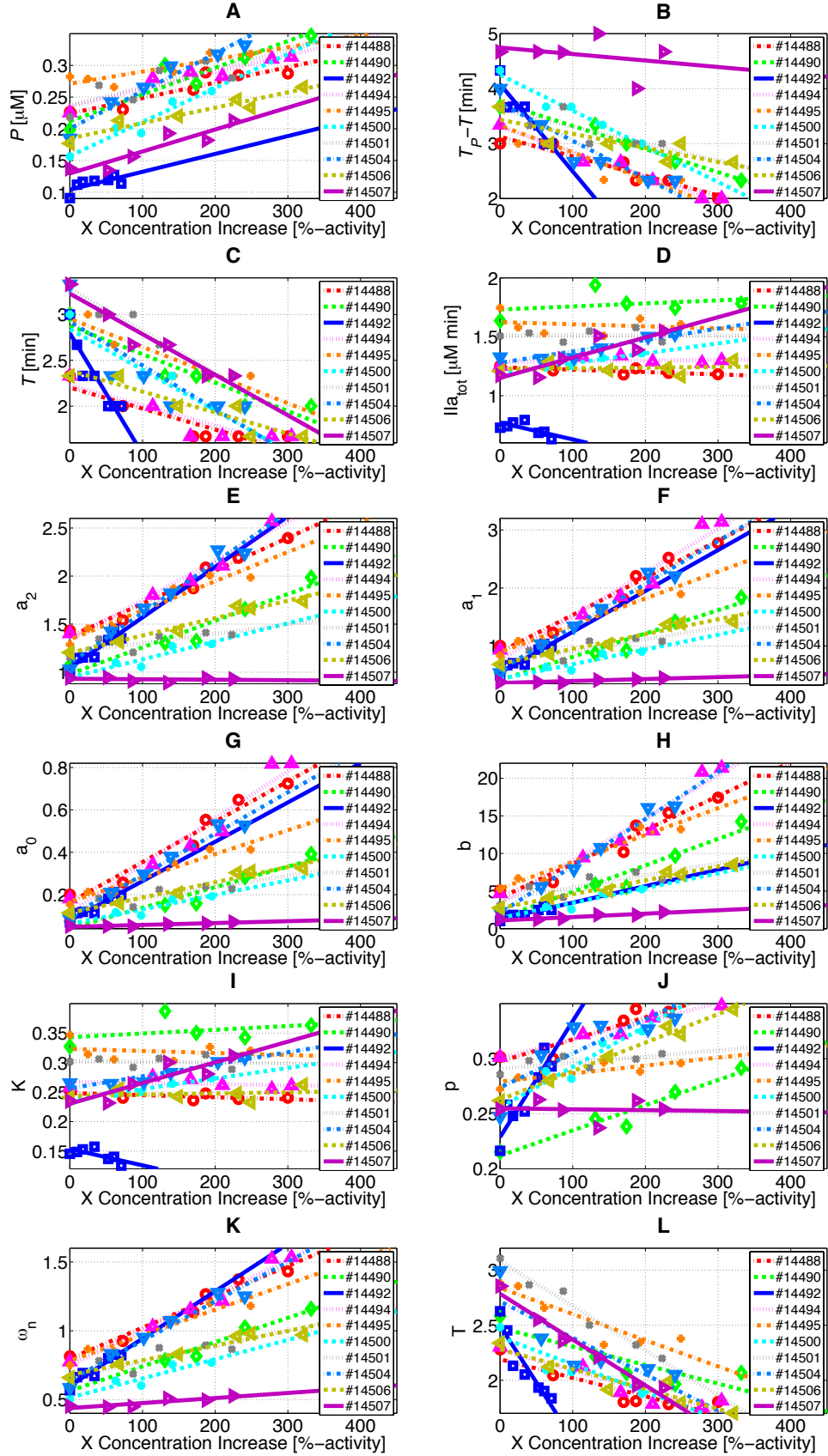


Fig. S13. Parameter effects caused by increasing the concentration of factor X in 10 normal plasma samples. In ten normal plasma samples, a concentration increase of factor X increases CAT peak thrombin concentration P (**A**), and decreases the rise time $T_p - T$ (**B**) and the delay T (**C**). The total thrombin produced Πa_{tot} (**D**) is unaffected. A concentration increase of factor X increases temporal parameters a_2 (avg. $R^2 = 0.89$ in 9 samples with a trend), a_1 (avg. $R^2 = 0.90$), a_0 (avg. $R^2 = 0.91$), and b (avg. $R^2 = 0.90$) in (**E**), (**F**), (**G**), and (**H**), respectively. An increase in factor X concentration does not affect the gain K (**I**), but the cut-off frequency p (avg. $R^2 = 0.81$ in 9 samples with a trend) (**J**) and the natural frequency ω_n (avg. $R^2 = 0.90$) (**K**) increase, while the SDO-fitted delay T (avg. $R^2 = 0.84$) (**L**) decreases.

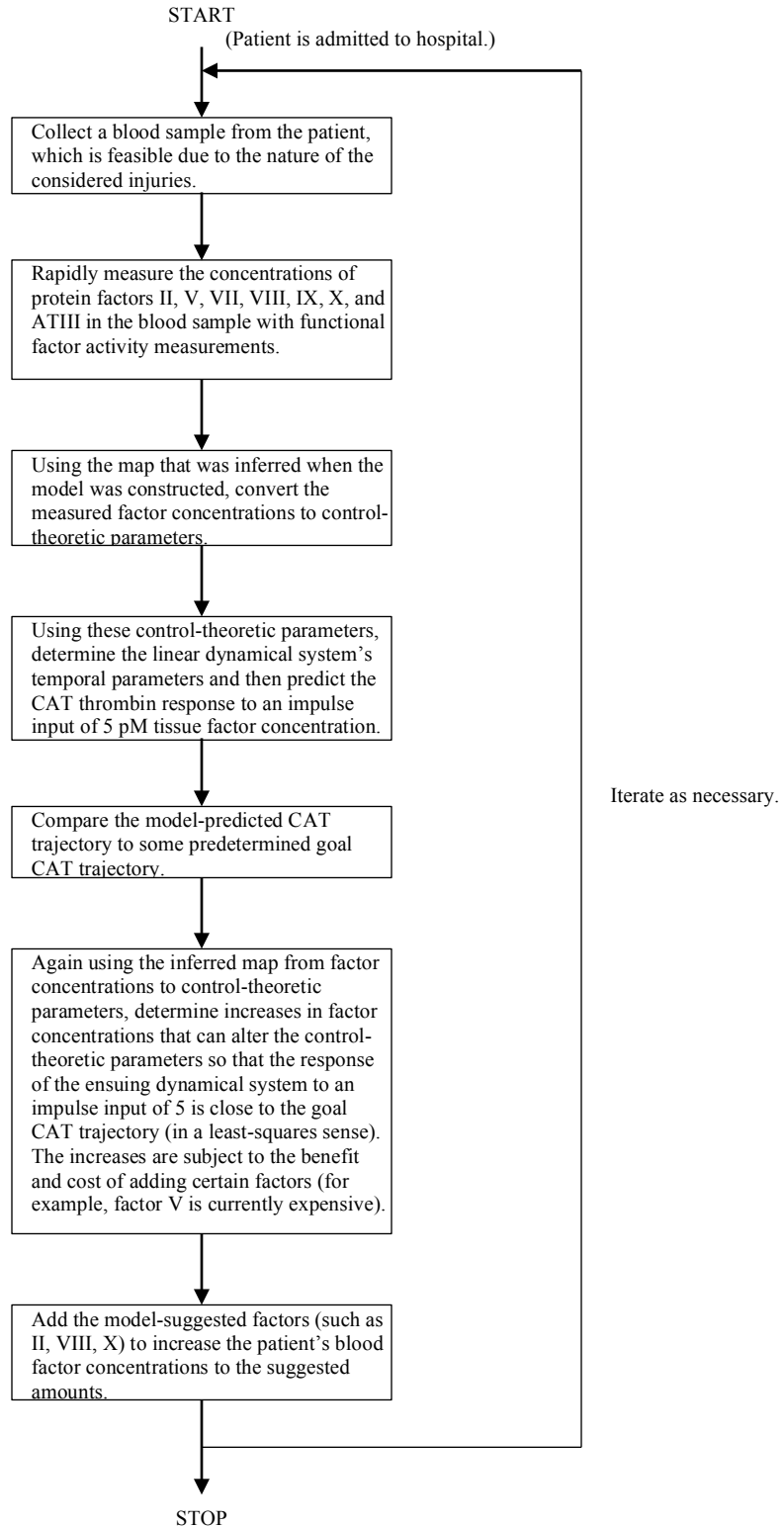


Fig. S14. Proposed clinical workflow.

Supplementary Tables

Table S1. Summary of trauma patient characteristics.

Characteristic	Mean \pm std. dev. or percentage (no. out of 40)
Age (years)	43.5 \pm 19.6
Male/female	85% (34) / 15% (6)
ISS	10.3 \pm 10.6
Blunt/penetrating injury	57.5% (23) / 42.5% (17)
TBI not present/present	75% (30) / 25% (10)
Alive/dead	90% (36) / 10% (4)
PTT (s)	27.8 \pm 3.7
PT (s)	14.0 \pm 1.4
INR	1.1 \pm 0.1

Table S2. Normal and trauma patient plasma sample data (provided as an Excel file). Demographic and injury characteristics of 40 trauma patients admitted to San Francisco General Hospital, measured CAT thrombin trajectory data for the 20 normal and the 40 trauma patient plasma samples after stimulating with 5 pM of tissue factor, measured concentrations of blood protein factors II, V, VII, VIII, IX, X, and ATIII in each normal and trauma sample, and fitted temporal and computed control-theoretic parameters of all CATs.

Table S3. Closeness of trauma patient factor concentrations to values from control mean plasma. In the table, -1 denotes a factor deficiency more than 10% of the respective factor concentration of control mean plasma, 0 denotes a factor within 10% of the respective factor concentration of control mean plasma, and 1 denotes a factor excess more than 10% of the respective factor concentration of control mean plasma.

ID	II	V	VII	VIII	IX	X	ATIII
Control mean plasma value	87	80	87	92	91	90	88
Control mean plasma range	78.3 - 95.7	72 - 88	78.3 - 95.7	82.8 - 101.2	81.9 - 100.1	81 - 99	79.2 - 96.8
2543	0	1	-1	1	1	-1	0
2575	0	0	-1	1	0	-1	1
2580	-1	0	-1	1	1	-1	-1
2597	-1	0	-1	1	0	-1	1
2624	-1	-1	-1	-1	0	-1	0
2634	-1	-1	-1	-1	1	-1	0
2665	0	0	-1	1	1	0	1
2668	0	1	1	1	1	1	1
2675	-1	-1	1	-1	-1	-1	-1
2711	-1	-1	-1	-1	1	-1	-1
2714	0	-1	-1	1	1	-1	0
2716	-1	-1	0	1	0	-1	-1
2743	-1	-1	1	-1	-1	-1	-1
2751	-1	-1	-1	-1	-1	-1	-1
2771	0	-1	1	0	-1	0	1
2772	-1	-1	0	-1	0	-1	-1
2784	0	0	-1	-1	1	0	0
2797	0	0	1	1	1	1	1
2814	0	-1	0	-1	-1	0	0
2816	-1	-1	-1	1	1	0	-1
2817	-1	-1	-1	-1	-1	0	-1
2819	-1	-1	1	-1	0	-1	0
2827	-1	-1	1	-1	-1	-1	-1
2829	-1	-1	-1	-1	-1	-1	0
2841	-1	-1	1	-1	0	-1	0
2843	-1	-1	0	-1	-1	-1	0
2860	-1	-1	1	0	-1	-1	0
2881	-1	-1	-1	0	1	-1	0
2883	1	0	-1	1	1	1	0
2885	-1	-1	-1	-1	-1	-1	-1
2892	0	-1	1	1	1	1	1
2924	1	-1	1	-1	1	-1	-1
2767	0	0	1	1	1	1	0
2818	0	-1	-1	-1	1	0	1
2830	0	-1	1	0	0	0	-1
2840	-1	-1	1	-1	-1	0	0
2872	0	-1	1	-1	1	0	1
2878	0	-1	-1	-1	0	-1	0
2895	-1	-1	1	0	-1	-1	0
2901	-1	-1	-1	-1	-1	-1	1

Table S4. Closeness of trauma patient factor concentrations to means from 20 normal plasma samples. In the table, -1 denotes a factor deficiency more than one standard deviation below the respective factor concentration mean of the 20 normal plasma samples, 0 denotes a factor within one standard deviation of the respective factor concentration mean of the 20 normal plasma samples, and 1 denotes a factor excess more than one standard deviation above the respective factor concentration mean of the 20 normal plasma samples.

ID	II	V	VII	VIII	IX	X	ATIII
Mean of 20 normal samples	78.7	50.7	81.6	32.5	115.2	74.6	83.3
One std. dev. range	67.1 - 90.3	34.4 - 66.9	63.8 - 99.4	25.0 - 40.0	91.9 - 138.5	61.5 - 87.7	73.2 - 93.4
2543	0	1	-1	1	1	0	1
2575	1	1	-1	1	0	0	1
2580	-1	1	-1	1	0	-1	0
2597	-1	1	-1	1	0	-1	1
2624	-1	0	-1	1	-1	-1	0
2634	-1	0	0	1	0	0	0
2665	0	1	0	1	0	1	1
2668	1	1	1	1	1	1	1
2675	-1	-1	0	1	-1	-1	-1
2711	0	-1	-1	0	0	0	-1
2714	0	-1	-1	1	1	0	0
2716	-1	0	0	1	0	-1	0
2743	-1	0	1	1	-1	0	0
2751	0	0	0	1	-1	0	0
2771	0	0	1	1	-1	0	1
2772	0	-1	0	1	-1	0	-1
2784	0	1	-1	0	0	1	0
2797	1	1	1	1	1	1	1
2814	0	0	0	1	-1	0	1
2816	0	0	0	1	0	0	0
2817	0	-1	0	1	-1	1	-1
2819	0	0	1	1	-1	0	0
2827	-1	-1	1	1	-1	-1	-1
2829	0	-1	0	1	-1	0	0
2841	0	-1	1	1	0	0	0
2843	-1	0	0	1	-1	0	0
2860	-1	0	1	1	-1	-1	0
2881	-1	-1	-1	1	0	-1	0
2883	1	1	-1	1	1	1	1
2885	0	-1	-1	1	-1	0	0
2892	0	0	1	1	1	1	1
2924	1	0	1	1	0	0	0
2767	0	1	1	1	0	1	1
2818	0	-1	-1	1	0	0	1
2830	0	-1	1	1	0	0	0
2840	0	0	1	1	-1	0	0
2872	0	0	1	1	1	1	1
2878	0	0	0	1	-1	0	0
2895	0	0	1	1	-1	0	0
2901	0	-1	0	1	-1	0	1

Table S5. Unsuccessful k-means classification of normal and trauma using four CAT dimensions.

ID. NO.	NORMAL (N) OR TRAUMA (T)	K-MEANS CLUSTER NO.
14488	N	1
14489	N	1
14490	N	2
14491	N	2
14492	N	1
14493	N	1
14494	N	1
14495	N	2
14496	N	1
14497	N	1
14498	N	2
14499	N	2
14500	N	2
14501	N	2
14502	N	1
14503	N	2
14504	N	2
14505	N	2
14506	N	2
14507	N	2
2543	T	1
2575	T	1
2580	T	1
2597	T	1
2624	T	1
2634	T	1
2665	T	2
2668	T	1
2675	T	1
2711	T	1
2714	T	2
2716	T	1
2743	T	1
2751	T	1
2771	T	1
2772	T	1
2784	T	2
2797	T	2
2814	T	1
2816	T	2
2817	T	2
2819	T	1
2827	T	1
2829	T	2
2841	T	2
2843	T	1
2860	T	1
2881	T	1
2883	T	2
2885	T	1
2892	T	2
2924	T	1
2767	T	2
2818	T	2
2830	T	2
2840	T	2
2872	T	2
2878	T	1
2895	T	1
2901	T	1

Table S6. Unsuccessful k-means classification of normal and trauma using seven concentrations, equivalent to using the first two and the first three principal components.

ID. NO.	NORMAL (N) OR TRAUMA (T)	K-MEANS CLUSTER NO.
14488	N	1
14489	N	1
14490	N	1
14491	N	1
14492	N	1
14493	N	1
14494	N	1
14495	N	1
14496	N	1
14497	N	1
14498	N	1
14499	N	1
14500	N	1
14501	N	1
14502	N	1
14503	N	1
14504	N	1
14505	N	1
14506	N	1
14507	N	1
2543	T	1
2575	T	1
2580	T	1
2597	T	1
2624	T	1
2634	T	1
2665	T	1
2668	T	1
2675	T	1
2711	T	1
2714	T	1
2716	T	1
2743	T	2
2751	T	1
2771	T	1
2772	T	1
2784	T	1
2797	T	2
2814	T	1
2816	T	1
2817	T	1
2819	T	1
2827	T	1
2829	T	1
2841	T	1
2843	T	1
2860	T	1
2881	T	1
2883	T	1
2885	T	1
2892	T	1
2924	T	2
2767	T	1
2818	T	1
2830	T	1
2840	T	1
2872	T	2
2878	T	1
2895	T	1
2901	T	1

Table S7. Conversion factors used for Hockin-Mann model prediction of trauma CATs.

Factor	Control mean plasma percentage	Hockin-Mann (<i>II</i>) initial concentration	Conversion factor (Hockin-Mann initial concentration / control mean plasma percentage)
II	87	$1.4 \times 10^{-06} \text{M}$	$1.61 \times 10^{-08} \text{M}$
V	80	$2.0 \times 10^{-08} \text{M}$	$2.50 \times 10^{-10} \text{M}$
VII	87	$1.0 \times 10^{-08} \text{M}$	$1.15 \times 10^{-10} \text{M}$
VIII	92	$7.0 \times 10^{-10} \text{M}$	$7.61 \times 10^{-12} \text{M}$
IX	91	$9.0 \times 10^{-08} \text{M}$	$9.89 \times 10^{-10} \text{M}$
X	90	$1.6 \times 10^{-07} \text{M}$	$1.78 \times 10^{-09} \text{M}$
ATIII	88	$3.4 \times 10^{-06} \text{M}$	$3.86 \times 10^{-08} \text{M}$

Table S8. Thrombin dynamical system linearity testing data (provided as an Excel file).

Three-trial measured CAT data resulting from stimulating a pool of non-injured plasma samples (different from the 20 normals) at various tissue factor concentrations, and the measured CAT data produced after stimulating the 20 normal plasma samples with 1 pM of tissue factor and 20 pM of tissue factor.

Table S9. Factor addition independence testing data (provided as an Excel file).
Measurements of the concentration of blood protein factors in normal plasma samples after an additional amount of a single factor was spiked in.

Table S10. Mean of the SD of nonspiked factor concentrations across multiple normal plasma samples.

Spiked	II	V	VII	VIII	IX	X	ATIII
II		6.4611	5.9633	6.8352	8.4848	4.9528	5.9496
VII	4.4170	4.2520		12.3619	8.0849	14.3469	5.0000
VIII	13.0065	5.8279	8.1578		15.9807	6.2259	4.6162
IX	7.8506	8.6765	7.3919	7.6297		3.7638	8.0828
X	15.3907	6.5694	8.4187	13.9994	7.6702		5.8404
ATIII	6.0472	5.3016	8.4857	4.4789	9.3742	14.2680	

Table S11. Maximum nonspiked factor concentration in normal plasma samples.

Normalization factor	II	V	VII	VIII	IX	X	ATIII
	206	155	203	178	281	300	175

Table S12. Factor perturbation data (provided as an Excel file). Measured CAT thrombin trajectory data for normal plasma samples spiked with one of the factors II, VIII, or X, measured concentrations of spiked factors, and fitted temporal and computed control-theoretic parameters of these CATs.

Table S13. Ancillary factor perturbation data and model validation data (provided as an Excel file).

CAT trajectories of normal plasma samples that were spiked with factor V at different tissue factor concentrations, CAT trajectories for normal plasma samples that were spiked with factors IX and ATIII individually, and CAT trajectory data and available factor concentration measurements for those normal and trauma plasma samples that were spiked with arbitrary concentrations of factors II, VIII, and X to validate this paper's model.